applied sciences

MDPI

Article

Quasi-Experimental Field Assessment of Haul-Road Maintenance Effects on Fuel Consumption, Cycle Time and Mechanical Loading of Open-Pit Dump Trucks

Aman Tulegenovich Shakenov [1], Assem Yerzhankyzy Utegenova [1,*], Ivan Nikitovich Stolpovskikh [1], Ainura Berikbolovna Orumbassarova [1], Boris V. Malozyomov [2] and Nikita V. Martyushev [3,*]

[1] Institute of Energy and Mechanical Engineering Named After A. Burkitbayev, Department of Technological Machines and Gas Turbine Installations, Satbayev University, Almaty 050013, Kazakhstan; ashakenov@yahoo.com (A.T.S.); i.stolpovskikh@satbayev.university (I.N.S.); a.orumbassarova@satbayev.university (A.B.O.)
[2] Department of Electrotechnical Complexes, Novosibirsk State Technical University, 20, Karla Marksa Ave., Novosibirsk 630073, Russia; borisnovel@mail.ru
[3] Department of Information Technologies, Tomsk Polytechnic University, Tomsk 634050, Russia
* Correspondence: a.utegenova@satbayev.university (A.Y.U.); martjushev@tpu.ru (N.V.M.)

Abstract

Haul-road condition in open-pit mining affects fuel consumption, transport-cycle throughput and dump-truck mechanical loading. This study conducted a quasi-experimental field assessment of local maintenance effects on severely degraded road segments. The full cycle register contained 32,000 entries, of which 30,808 passed quality control and were used for background engineering characterization. The primary difference-in-differences (DiD) analysis used 2634 matched-control cycle–focal-segment observations, while 72,000 one-second telemetry records formed a separate 20 h dynamic validation subset. Relative to matched-control dynamics, maintenance increased RCI by 3.26 points and reduced IRI by 6.24 m/km, the apparent rolling-resistance descriptor by 2.71 percentage points and rut depth by 41.2 mm. Regression-adjusted effects were −10.6 L/cycle for fuel, −0.78 min for cycle time, +10.7 km/h for segment speed, −0.351 g for vibration RMS and −78.2 MPa-eq. for the suspension-stress proxy. A 14-day lead-placebo/event-time diagnostic found no detectable pre-intervention divergence, and non-negative cohort-weighted group-time ATT estimates closely matched the TWFE results. The coefficients are interpreted as site-specific local intervention-window effects rather than annual fleet-wide constants.

Keywords: open-pit mining; haul-road maintenance; UAV/LiDAR profiling; dump truck telemetry; fuel consumption; cycle time; mechanical-load proxy; difference-in-differences; rolling-resistance descriptor

Academic Editor: Valentin L. Popov

Received: 10 July 2026
Revised: 30 July 2026
Accepted: 3 August 2026
Published: 4 August 2026

1. Introduction

The open-pit transport system is one of the most energy-intensive and capital-intensive circuits of open-pit mining. Even with the same productivity of the excavator-loading section, the actual throughput of the open pit may decrease due to the deterioration of the condition of technological roads: the growth of unevenness, rutting, local defects in the pavement, deterioration of drainage and an increase in rolling resistance [1–3]. In such conditions, the road infrastructure ceases to be a passive element of the production scheme and becomes a controllable factor in fuel consumption, cycle time, travel speed and mechanical load of the undercarriage of a mining dump truck.

Existing studies on the digitalization of open-pit mining, the analysis of truck-haulage systems and telemetry of quarry transport confirm the relevance of multi-source data, but a significant part of the work considers road parameters, the operating cycle and the mechanical response of the machine separately [4–6]. Therefore, there is a methodological gap between measuring the geometric condition of a technological road and quantifying how the repair of a particular segment changes the operation of the transport cycle relative to the control dynamics.

In the works devoted to the monitoring of technological roads and unmanned surveying tools, it is shown that UAV/LiDAR, digital road profiles and mobile sensors make it possible to move from visual inspection of defects to a parametric description of the road profile, unevenness, rutting and local zones of pavement failure [7–9]. However, the geometric and indexation indicators of the road themselves do not answer the main engineering question: what measurable losses do they cause in fuel, cycle time and mechanical load of the transport vehicle.

A separate group of studies looks at rolling resistance, road bumps, fuel consumption and performance of transport vehicles. Studies on quarry roads show that rolling resistance can be estimated from the operational data of dispatching systems [10]. Work on road unevenness and energy dissipation of transport vehicles additionally confirms that the condition of the profile, slope, weight of the load and the mode of movement form the energy penalty of the transport cycle [11–13]. However, in most cases, the impact of road conditions is estimated as a regression relationship, a physical model or an operational correlation, while quasi-experimental comparison of repaired and control sections is used much less frequently.

The resource component in such systems should be interpreted carefully. The long-term reliability of mining dump trucks requires separate statistics of failures by nodes, time to event, censorship and seasonal recurrence of observations [14,15]. In this paper, therefore, it is not the total failure of the machine that is analyzed, but a narrower and more directly measurable loop: vibration RMS, suspension-stress proxy, road-sensitive maintenance events and downtime intensity as indicators of road-induced mechanical-load risk.

Related studies on monitoring with low-cost sensors, recognition of road defects, assessment of road surface unevenness, and safety of mining machines demonstrate the maturity of the sensor base and algorithmic tools [16,17]. However, the transfer of these approaches to heavy mining dump trucks requires taking into account a different weight of the vehicle, a different suspension stiffness, a different rolling resistance structure and a significantly higher cost of a road maintenance error.

Work on UAV/AI tools and drone-based monitoring of mining sites shows a transition from one-time surveys to regular digital monitoring of the site condition [18,19]. Reviews on digital twins and predictive maintenance in mining operations emphasize that such data are increasingly used for asset management, but require a separate description of the measurement layer, statistical evaluation, and engineering solution [20,21]. For open-pit mines, research on fuel-efficient road classification and reliability-oriented analysis of mining dump truck assemblies is also important [22–24]. Work on forecasting fuel consumption confirms the sensitivity of truck-haulage systems to road conditions, load and driving mode [25,26].

Energy and transport-logistics studies of mining dump trucks show that the magnitude of the effect depends on the class of the machine, the operating cycle and the scheme of delivery of rock mass [27–29]. Sensor digitalization of quarries and methods for recognizing road defects form the basis for more frequent monitoring of the condition of technological roads [30–32]. For road surfaces and mobile monitoring, the applicability of device-based IRI/roughness assessment was additionally shown, which is methodically close to the problem of segment profile control [33–35]. Studies of roughness-induced vehicle energy dissipation have linked road bumps to energy losses and vibration excitation of the vehicle [36,37].

The paper analyzes the observed field intervention: repair and profiling work on problem road segments. Predictive and interpretive analytics are assigned to the downstream engineering layer after quasi-experimental before–after/matched-control evaluation.

The key methodological transition is to abandon the simple regression dependence "bad road—high fuel consumption" in favor of a scheme that separates the effect of road intervention and background variability associated with weather, changes in load, queues, shifts, individual characteristics of cars and routes. For this purpose, each repaired segment is associated with a control segment, and for both groups, the intervals before and after the control date are allocated, and the first days after the repair are excluded as a washout period.

The scientific idea of the work is that the technological road is considered not as a passive background factor, but as a controlled intervention object in the system "road—dump truck—transport cycle—mechanical loading". In this system, the deterioration of IRI, RCI, rutting and rolling resistance forms a cascade of measurable operating effects: reduced speed, longer cycle times, increased fuel consumption, increased vibration and increased stresses in the suspension elements.

The purpose of the study was to perform a quasi-experimental field assessment of the local effect of the repair of technological roads on the fuel consumption of trips that passed the analyzed segment, the duration of the corresponding transport cycle, the speed of the focus segment, RMS vibration and the suspension-stress proxy of mining dump trucks. Methodologically, the goal is limited to selected high-severity intervention segments: the obtained coefficients are not interpreted as an average annual effect for the entire fleet or the entire open-pit road network.

The main contribution of the work is to combine independent measurement of road condition, operational response of the transport cycle and quasi-experimental assessment of the repair intervention relative to control segments. This makes it possible to separate the local field effect of repair from the background variability associated with weather, cargo weight, slope, shift, individual characteristics of vehicles and route structure.

The scientific novelty of the study lies in the assessment of the effect of maintenance of quarry technological roads as a field-supported intervention effect under matched-control and pre-trend assumptions, and not as a simple correlation between unevenness and fuel consumption. The measured change in the road profile is compared with the change in the fuel, time, speed and mechanical response of the trucks in the intervention and control observation windows.

Reference [38] was produced by the same author team and used the same industrial monitoring context, but it addressed a different question. That study quantified observational associations among haul-road degradation, fuel-use proxy burden, dynamic response and transport-cycle stability. It did not evaluate repair events through matched controls, washout windows, event-time diagnostics, lead-placebo analysis or group-time ATT. The present manuscript therefore reuses the monitoring infrastructure while constructing a distinct 2634-observation intervention-window sample and estimating the local effect of maintenance rather than another road-condition association.

2. Theoretical Framework and Conceptual Model

The conceptual framework treats haul-road maintenance as a segment-level intervention that first changes independently measured road-state variables and then propagates through operational mediators to energy, production and mechanical-response outcomes.

The hypothesized primary pathway is: maintenance intervention → improvement in RCI, IRI, rut depth and the apparent rolling-resistance descriptor → stabilization of segment speed and reduction in forced braking or gear shifting → lower fuel use, cycle time, vibration RMS and suspension-stress proxy. This ordering prevents truck-response variables from being used to construct the road-condition exposure.

The core outcomes were selected to represent four non-equivalent engineering domains. Fuel consumption is the energy outcome; cycle time is the production-throughput outcome; segment speed is the local operational mediator and response; and vibration RMS together with the suspension-stress proxy quantify the short-window dynamic-load burden. Their simultaneous use is therefore not a repetition of one response variable but a test of whether the intervention produces a physically coherent multichannel effect.

Observed confounding is addressed through payload, grade, rainfall, wetness, queue/idle context, route and shift information, together with truck, segment and event-period fixed effects. Potentially unobserved factors include operator behavior, local traffic conflicts, unrecorded loading delays, hidden pavement or subgrade conditions, and variation in repair execution. These factors cannot be eliminated by the observational design; consequently, the manuscript uses the terms "field-supported local intervention effect" and "quasi-experimental estimate" rather than randomized causality.

Tire temperature, cumulative brake wear and component failure rate were not specified as primary outcomes because the available industrial records did not provide continuous synchronized measurements or a sufficiently long and component-resolved failure denominator for these variables. Braking events and road-sensitive maintenance records are retained only as supporting indicators. Microseismic monitoring addresses a different pathway—internal rock-mass fracture and dynamic-hazard evolution—and is therefore considered a complementary future data layer rather than a substitute for haul-road and truck-response measurements.

Figure 1 formalizes the causal pathway, separates directly measured variables from operational mediators, and identifies both observed controls and residual unobserved confounding.

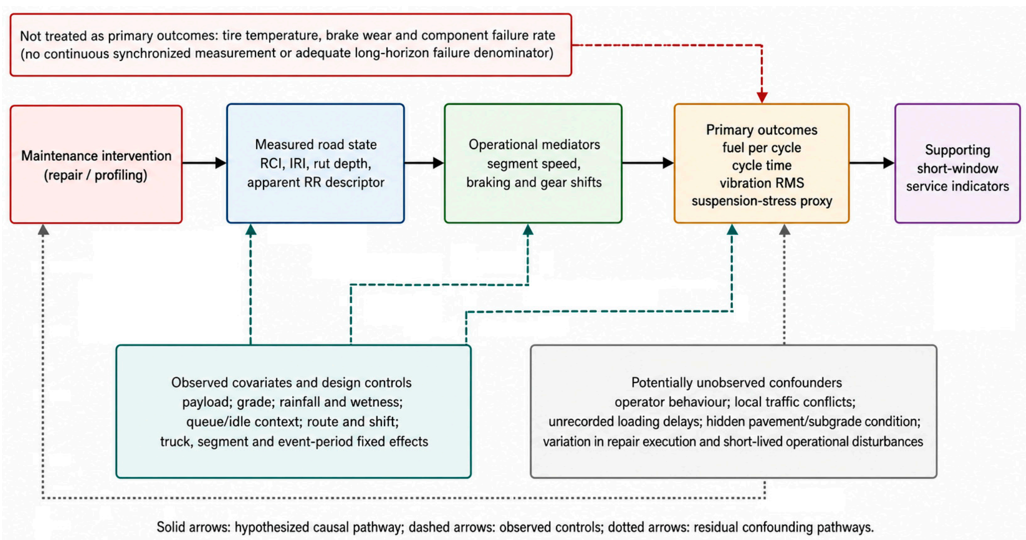

Figure 1. Conceptual causal framework for the field assessment of haul-road maintenance. Solid arrows denote the hypothesized causal pathway, dashed arrows denote observed controls, and dotted arrows denote residual confounding pathways.

The diagram defines the interpretation boundary used throughout the study. Road-state variables are measured independently of the truck outcomes; the DiD estimand is applied to the intervention–control contrast; and short-window service indicators are interpreted as mechanical-load-risk evidence rather than as direct proof of long-term reliability improvement.

3. Materials and Methods

3.1. Study Site, Fleet and Analytical Data Layers

The study was carried out for the open-pit vehicle system of the Ekibastuz coal mine. The cycle register contained 32,000 transport cycles from 1 January to 31 December 2024; after multi-stage quality control, 30,808 valid records were retained. The monitored fleet included 12 Caterpillar 785D-class mining trucks. Statistical models used the actual mass of the load at the cycle level rather than the rating value. The road network was represented by 12 segments, distributed over 4 main route contours.

The data were organized into distinct but linked analytical layers. The full valid cycle-level register was used for descriptive characterization and physical consistency checks. The primary intervention effect was estimated in matched-control DiD windows. The unit of analysis was the cycle–focal-segment observation: fuel and cycle time describe the complete trip traversing the focal segment, whereas speed, vibration and the suspension-stress proxy describe the local segment passage.

Cycle-level records were obtained from the operator's dispatch, VIMS and maintenance-log systems; road-condition variables were obtained from UAV/LiDAR surveys and field inspections; and the weather layer was used as an external control. Truck, trip and service-event identifiers were anonymized. Source integration used cycle_id, truck_id, route_id, segment_id, timestamps and GPS chainage, with all rejected joins retained in the QA log.

Figure 2 summarizes the revised quasi-experimental data architecture and explicitly separates the full observational cycle registry, the matched-control DiD estimation window and the limited 1 Hz telemetry validation subset.

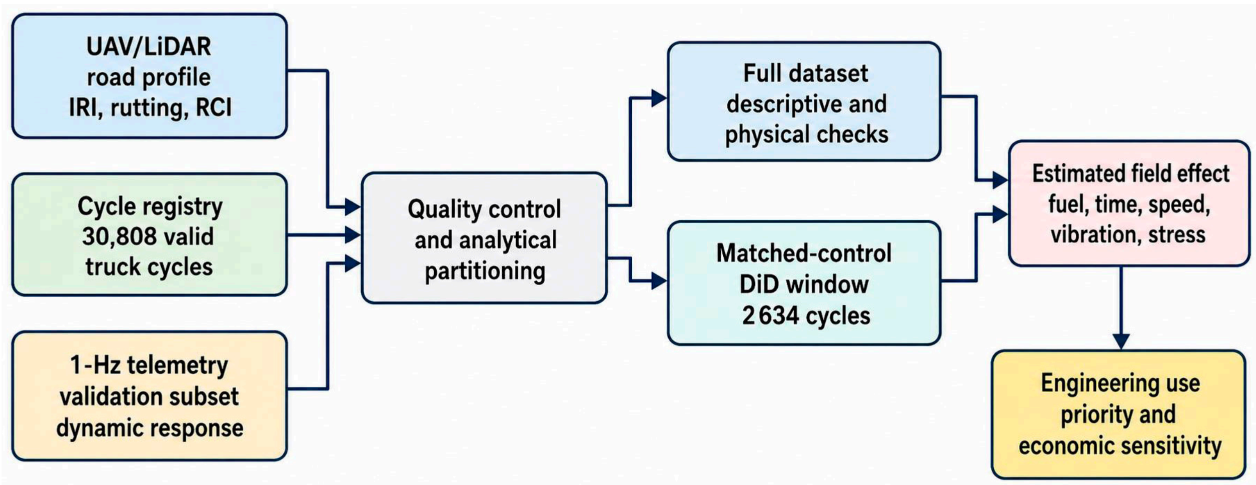

Figure 2. Quasi-experimental data architecture linking UAV/LiDAR road profiling, cycle-level telemetry, matched-control DiD estimation and engineering interpretation.

Figure 2 distinguishes the three analytical denominators. The full register and the 1 Hz subset support background characterization and dynamic plausibility checks, respectively, whereas the repair effect is estimated from 2634 observations in the matched-control DiD windows. The three layers are linked for traceability but are not pooled as if they represented the same sampling frequency.

3.2. Before-And-After Design with Selected Control Segments

Five road segments with pronounced profile degradation were included in the intervention group. For each of them, a control segment was selected without road intervention in the corresponding observation window. The selection was carried out according to the route contour, transport role, longitudinal slope range, length of the section, traffic intensity and stability of the pre-repair trend. Control segments shall not be treated as physically identical copies of the areas to be repaired; their function is to assess the background calendar and operational dynamics that could have been observed without repairs.

Figure 3 presents the intervention–control pairing logic and the event-time structure used to separate pre-intervention, washout and post-intervention observations.

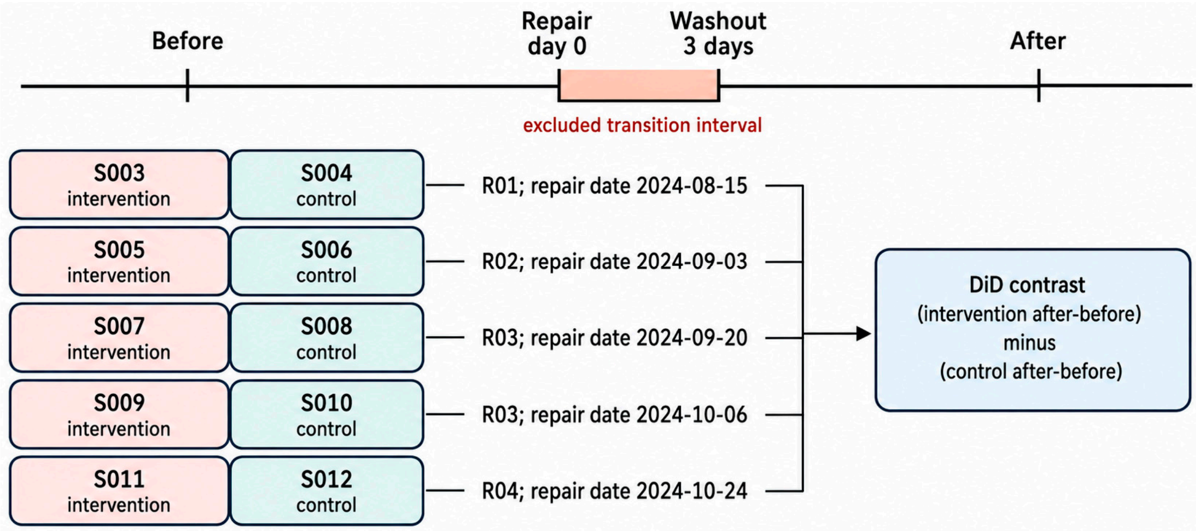

Figure 3. Intervention–control pairing and event-time structure used for haul-road maintenance assessment.

Figure 3 clarifies the quasi-experimental design. The analysis includes only observations before the intervention and after the end of the washout interval. The first three days after the repair are excluded, since during this period transient effects of pavement compaction, changes in traffic organization and local stabilization of the profile are possible.

3.3. UAV/LiDAR Profiling and Road Condition Survey

The road surface was described based on UAV/LiDAR profiling and inspection data. The field measurement circuit followed the engineering diagram of the DJI Matrice 300 RTK (SZ DJI Technology Co., Ltd., Shenzhen, China) with the Zenmuse L1 LiDAR (SZ DJI Technology Co., Ltd., Shenzhen, China) payload and RTK/PPK trajectory control. The array of 10,320 profile points corresponds to repeated surveys for 12 monitored segments, rather than a single longitudinal passage of the road network. With a total length of about 12.84 km, a 5 m step gives approximately 2568 points for one full shooting round.

RCI is interpreted as a road condition index on a scale of 0–10, where a higher value corresponds to the best condition of the segment. After the repair, RCI is expected to increase with a simultaneous decrease in IRI, apparent rolling-resistance descriptor, rutting and density of local defects. The direction of these indicators is set before the calculation of operational effects.

The UAV/LiDAR circuit was used as an independent measuring source of road condition. The IRI and rutting calculations were performed after filtering out single outliers, checking the continuity of the longitudinal profile, matching the chainage and interpolating the profile to a single 5 m pitch. Rolling resistance in the article is interpreted as a segment-date engineering estimate obtained from the combination of road inspection, profile, humidity class and operational protocol of the quarry. This is not a direct dynamometer measurement of rolling resistance force. Road signs are not derived from fuel consumption, speed, vibration or suspension-stress proxy.

Figure 4 demonstrates a representative UAV/LiDAR longitudinal profile before and after maintenance and illustrates how segment-level indices are connected with the along-road geometry of the repaired section.

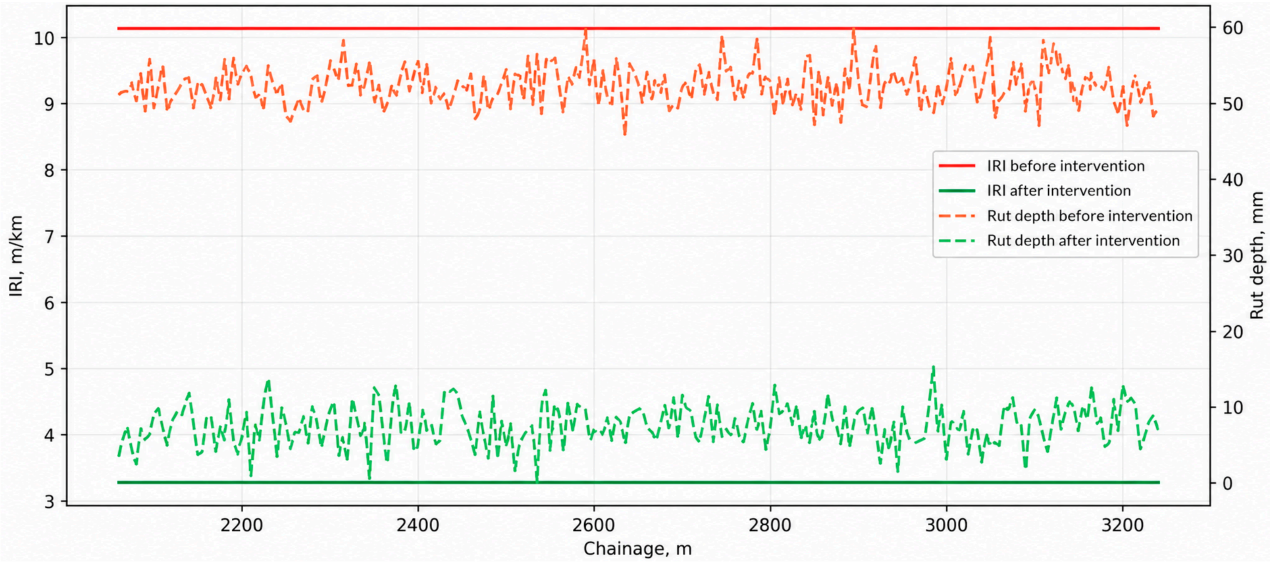

Figure 4. UAV/LiDAR longitudinal profile of IRI and rut depth before and after maintenance for representative segment S003.

Figure 4 shows that segment recovery is manifested not only in the integral growth of the RCI, but also in the longitudinal profile structure: after repair, local IRI peaks and rut depth decrease. This provides the physical basis for subsequent analysis of the truck's fuel, speed and mechanical response.

3.4. Cycle-Level Telemetry and the 1 Hz Dynamic Subset

The cycle register included trip start and end time, route, focus road segment, dump truck, shift, load weight, distance, segment speed, cycle duration, queue, idle time, fuel consumption per cycle, route-normalized consumption per tonne-kilometer, engine load, gear shifts, braking events, acceleration, RCI, IRI, the apparent rolling-resistance descriptor, rutting, pothole density, RMS vibration, suspension-stress proxy, pressure in tires, air temperature, precipitation and road humidity. Operational records were provided by the site operator in an anonymized form from dispatch/VIMS/maintenance-log circuits. Truck and trip identifiers were used only for grouping and to control recurrence.

The 1 Hz telemetry subset comprised 72,000 one-second records, equivalent to approximately 20 h of instrumented focal-segment passages. A pass was retained only when timestamps were monotonic, the modal sampling interval was 1 s, at least 95% of expected records were present, GPS chainage was continuous, cycle_id and segment_id were consistent, and both pre- and post-maintenance phases were represented. The subset was used only to verify the dynamic form of changes in speed, vibration, braking and the stress proxy along repaired chainage; DiD coefficients were estimated from the cycle-level register.

3.5. Multi-Source Synchronization, Spatial Matching and Quality Control

The sources were first converted to a common mine-local time base. Cycle records were treated as event-level observations, the dynamic subset as a 1 Hz stream, road profiles as repeated 5 m chainage measurements, weather as a segment-date layer, and maintenance records as time-stamped truck events. Clock consistency was checked against cycle start/end boundaries and segment entry/exit times. A 1 Hz pass was flagged when a timestamp gap exceeded 2 s and was excluded when missingness exceeded 5% or when a discontinuity prevented reliable chainage reconstruction.

Spatial matching used the surveyed segment centerline and chainage. Telemetry points were assigned to a segment only when route direction, segment polygon and chainage order agreed; conflicting segment_id/GPS assignments were rejected. UAV/LiDAR profiles were interpolated to the common 5 m chainage grid after isolated-point filtering and continuity checks. A road-state survey was linked only within the corresponding pre- or post-repair phase; values were not interpolated across the intervention date.

Primary outcomes were analyzed by complete cases and were not imputed. Duplicate cycle_id records, non-monotonic timestamps, impossible route sequences and values outside equipment- or operation-specific physical ranges were excluded. Remaining continuous anomalies were screened within truck–route strata using a robust median/MAD rule and were reviewed rather than automatically deleted. Sensor plausibility checks compared GPS speed with segment distance divided by traversal time, fuel use with counter increments, and vibration channels with saturation and zero-variance criteria.

After these checks, 30,808 of 32,000 cycle records remained valid (96.3%). The weather layer contained 4392 segment-date records (366 days $\times$ 12 segments), and the QA log contained 1312 entries documenting exclusions, join conflicts, manual reviews and acceptance status. This workflow separates synchronization, spatial linkage, anomaly screening and analytical-sample assignment instead of treating data fusion as an unspecified aggregation step.

3.6. Targets and Quasi-Experimental Statistical Assessment

The primary outcomes were fuel consumption per cycle for trips traversing the focal segment, route-normalized fuel intensity, cycle time, segment traversal speed, vibration RMS and the suspension-stress proxy. Fuel and time represent energy and production consequences; speed is the direct local operational response; and vibration RMS and the suspension-stress proxy characterize dynamic mechanical loading. The stress variable is an engineering telemetry proxy and is not interpreted as a direct strain-gauge measurement.

For each indicator, the intrasegment change between the after and before periods was first calculated:

$$\Delta Y_i \;=\; \mathrm{mean}(Y_i \mid \mathrm{after}) - \mathrm{mean}(Y_i \mid \mathrm{before}) \tag{1}$$

where ΔY_i is the within-segment change; Y_i|after and Y_i|before are the corresponding post- and pre-intervention means. Negative values indicate improvement for fuel use, cycle time, vibration, stress proxy, IRI and rolling resistance; positive values indicate improvement for RCI and segment speed.

The main assessment of the effect was built as difference-in-differences, that is, the change in the intervention segments was compared with the background change in the control segments [38–40]:

$$\begin{aligned} DiD \;=\; &[\mathrm{mean}(Y \mid \mathrm{intervention}, \mathrm{after}) - \mathrm{mean}(Y \mid \mathrm{intervention}, \mathrm{before})] - \\ &-[\mathrm{mean}(Y \mid \mathrm{control}, \mathrm{after}) - \mathrm{mean}(Y \mid \mathrm{control}, \mathrm{before})] \end{aligned}, \tag{2}$$

where the first bracket is the post-minus-pre change for repaired segments and the second bracket is the corresponding change for matched controls. This definition fixes the sign convention and makes the estimand a change-in-changes rather than a difference between post-intervention levels.

The adjusted specification included segment, event-period/date and truck fixed effects together with production covariates. Because treatment status is time invariant at segment level, its main effect is absorbed by segment fixed effects; the identified parameter is the Treatment × Post interaction. Repeated observations were handled through clustered inference and wild-bootstrap confidence intervals rather than by treating all cycles as independent [41–43].

$$Y_{cst} = \alpha_s + \lambda_t + \kappa_k + \beta(Treat_s \times Post_t) + \gamma' X_{cst} + \varepsilon_{cst}, \tag{3}$$

where Y_{cst} is the outcome for cycle c, segment s and period t; α_s, λ_t and κ_k are segment, event-period and truck fixed effects; $Treat_s \times Post_t$ identifies repaired-segment observations after the intervention; X_{cst} contains payload, grade, rainfall, wetness and queue/idle controls; β is the local *DiD* coefficient; and ε_{cst} is the residual.

This specification avoids collinearity between $Treat_s$ and segment fixed effects and is consistent with the matched-control design. Cluster-robust and wild-bootstrap intervals account for dependence within segment pairs and for the small number of intervention groups.

Two additional robustness checks were specified. First, a lead-placebo cutoff was placed 14 days before each actual repair date, so that both pseudo-pre and pseudo-post observations came entirely from the true pre-intervention period. A 30-day lead was not feasible within the prespecified 21-day pre-window without changing the analytical sample. Second, segment-specific cohort-time effects were aggregated with non-negative post-window observation weights to obtain a group-time ATT comparison with the TWFE estimate [39,40].

The economic block is made as a scenario recalculation of the already estimated fuel reduction and cycle time into an engineering sensitivity:

$$S_{\text{gross}} = \Delta F \cdot N_{\text{cycles}} \cdot C_{\text{diesel}} + \frac{\Delta T \cdot N_{\text{cycles}} \cdot C_{\text{truck-hour}}}{60}, \tag{4}$$

where S_{gross} is the annualized scenario benefit per dump truck for comparable trips; ΔF is the estimated fuel reduction, L/cycle; ΔT is the cycle-time reduction, min/cycle; N_{cycles} is the annual number of comparable trips; C_{diesel} is the diesel price; and $C_{\text{truck-hour}}$ is the operating cost per truck-hour. This calculation is an engineering sensitivity analysis rather than a universal economic coefficient.

Physical Normalization and Indicators of Mechanical Load

For physical interpretation, the quasi-experimental estimate is supplemented by a normalization layer linking road geometry, rolling resistance, vehicle mass and mechanical response. This layer verifies dimensional consistency and the expected direction of effects; it is not used as a substitute for measured cycle outcomes.

$$L_j = \frac{l_i}{1000}, \tag{5}$$

where L_j is the focal-segment length in kilometers for cycle–segment observation j and l_i is the segment length in meters. This conversion permits consistent comparison of segments with different chainage lengths.

In all formulas in this subsection, the index j denotes the observation "cycle-focus segment" and is not a unit of time. Seconds are used only when describing a 1 Hz telemetry subset.

$$FI_j = \frac{F_j}{P_j \cdot D_{\text{cycle},j}}, \tag{6}$$

where FI_j is route-normalized fuel intensity, L/(t·km); F_j is cycle-level fuel use, L/cycle; P_j is actual payload, t; and $D_{\text{cycle},j}$ is full trip distance, km. Because fuel is recorded at cycle level, FI_j characterizes trips traversing the focal segment and is not interpreted as fuel consumed only within the repaired chainage.

$$RR_{\text{severity},j} = \frac{RR_{\text{descriptor},j}}{100}; \quad F_{RR,\text{interpret},j} = m_j \cdot g \cdot RR_{\text{severity},j}, \tag{7}$$

where $RR_{\text{severity},j}$ is the dimensionless apparent rolling-resistance descriptor, $RR_{\text{descriptor,j}}$ is the corresponding engineering descriptor in percent, and $F_{RR,interpret,j}$ is a dimensional interpretive quantity. It is not a direct drawbar-pull or wheel-force measurement and is not used as an independently measured response in the DiD regression.

The total estimated weight of the dump truck in the observation was given as

$$m_j = m_{\text{empty}} + P_j + m_{\text{fuel},j}, \tag{8}$$

where m_{empty} is empty-truck mass, P_j is actual payload and $m_{\text{fuel},j}$ is fuel mass. When continuous total-mass measurement is unavailable, this identity is used only for physical interpretation; statistical inference remains based on measured cycle-level outcomes.

$$F_{G,j} = m_j \cdot g \cdot \sin\left(\arctan\left(\frac{G_j}{100}\right)\right), \tag{9}$$

where $F_{G,j}$ is the grade-resistance component, and G_j is longitudinal grade, %. The expression establishes the expected mechanical direction of the grade effect; quantitative conclusions are obtained from the adjusted observational model.

$$E_{\text{road},j} = (F_{RR,\text{interpret},j} + F_{G,j}) \cdot s_j, \tag{10}$$

where $E_{\text{road},j}$ is the interpretive road-related energy component, J; s_j is focal-segment length, m; $F_{RR,\text{interpret},j}$ is the apparent rolling-resistance component; and $F_{G,j}$ is grade resistance. The expression is a dimensional consistency check and not an independent force validation.

The suspension-stress proxy was constructed as an MPa-eq. engineering scale rather than as direct structural stress. Its inputs were restricted to channels available before segment-level aggregation: vibration RMS, vibration 95th percentile, payload, segment speed, IRI, rut depth and the apparent rolling-resistance descriptor. The normalized construction is given below.

$$\begin{aligned} &MLI_c = 0.30 \cdot z(VIB_{RMS,c}) + 0.20 \cdot z(VIB_{95,c}) + 0.15 \cdot z(Payload_c) + 0.10 \cdot z(Speed_c) + \\ &+ 0.15 \cdot z(IRI_{s,t}) + 0.05 \cdot z(RutDepth_{s,t}) + 0.05 \cdot z(RRdescriptor_{s,t}), \\ &SSproxy_c = \sigma_{ref} + k_{proxy} \cdot MLI_c, \end{aligned} \tag{11}$$

where MLI_c is the dimensionless mechanical-load index; $VIB_{RMS,c}$ and $VIB_{95,c}$ are the median and 95th-percentile vibration responses; $Payload_c$ and $Speed_c$ describe exposure and operating state; $IRI_{s,t}$, $RutDepth_{s,t}$ and $RRdescriptor_{s,t}$ are road-state variables; σ_{ref} is the low-load reference level; and k_{proxy} converts the normalized MLI to the MPa-eq. proxy scale.

The weights are a prespecified engineering-priority score, not PCA coefficients and not parameters fitted to the repair outcome. Because all inputs are z-standardized, 0.30 + 0.20 assigns 50% to direct vibration response, 0.15 + 0.10 assigns 25% to exposure/operating state, and 0.15 + 0.05 + 0.05 assigns 25% to independently measured road condition. The weights were fixed before the before–after comparison to avoid outcome leakage. The MLI remains a secondary composite; the principal mechanical conclusion is also supported independently by the measured vibration RMS response.

For quasi-experimental interpretation, the assumption of conditional comparability of the dynamics of the repaired and control segments is adopted:

$$E[Y_{0,\text{after}} - Y_{0,\text{before}} \mid \text{Repair} = 1, X] = E[Y_{0,\text{after}} - Y_{0,\text{before}} \mid \text{Repair} = 0, X], \quad (12)$$

where $Y(0)$ is the potential outcome without road intervention; Repair = 1 denotes a repaired segment; Repair = 0 denotes its matched control; and X is the observed covariate vector. This conditional parallel-trends assumption supports quasi-experimental interpretation but does not imply randomized assignment.

$$\text{Bootstrap CI}_{95}(\theta) = [q_{0.025}(\theta^*), q_{0.975}(\theta^*)], \quad B = 1000, \quad (13)$$

where θ is the estimated effect, θ^* is a bootstrap replication, and $q_{0.025}$ and $q_{0.975}$ are empirical bootstrap quantiles. B = 1000 wild-bootstrap replications were used as a conservative supplement to cycle-level cluster-robust inference [42,43].

$$Priority_i = w_F \cdot N(\Delta FI_i) + w_T \cdot N(\Delta T_i) + w_M \cdot N(\Delta MLI_i) + w_R \cdot N(RRdescriptor_i), \quad (14)$$

where $Priority_i$ is the segment-level maintenance-priority score; ΔFI_i, ΔT_i, ΔMLI_i and $RRdescriptor_i$ represent the fuel, time, mechanical-load and road-resistance penalties; $N(\cdot)$ maps each component to [0, 1]; and the scenario weights sum to one. The score is used only after the statistical effect assessment.

The causal-estimation and prioritization layers are intentionally separated. DiD and regression adjustment estimate the local intervention effect, whereas $Priority_i$ converts already estimated penalties into an operational screening score. The priority matrix is therefore a decision-support visualization, not an additional causal or predictive model.

After describing the design scheme, the structure of the initial array, the passport of road segments and matched-control windows are given in Tables 1–5. These tables show which data is used for general physical validation, which data is used for DiD scoring, and which is used for dynamic 1 Hz telemetry confirmation.

Table 1. Analytical data layers and use after quality control.

Data Layer/Measurement Source	Volume, Traceability and Analytical Use
Observation period	1 January 2024–31 December 2024; used for seasonal and operational context.
Raw cycle-level registry	32,000 records before QC.
Valid cycle records	30,808 records after QC (96.3%); used for background calibration and physical consistency checks, not as the direct DiD effect sample.
Review/excluded records	635 review records and 557 excluded records retained only in the QC log.
DiD estimation window	2634 observations in matched-control before–after windows; primary sample for local field-effect estimates.

Table 1. *Cont.*

Data Layer/Measurement Source	Volume, Traceability and Analytical Use
Dump trucks	12 Caterpillar 785D-class trucks; identifiers anonymized; truck fixed effects included in adjusted models.
Payload handling	Nominal class used only for fleet description; actual payload measured at cycle level and used as a covariate.
Routes/road segments	4 route contours/12 monitored road segments.
Intervention/control segments	5 repaired segments/5 matched-control segments; two additional baseline segments used for background context.
UAV/LiDAR profile points	10,320 profile points from repeated survey rounds at 5 m chainage spacing; approximately four full road-network survey equivalents, used independently from truck-response variables.
Road-condition surveys	324 surveys; RCI, IRI, rolling resistance, rut depth and defect descriptors.
1 Hz telemetry subset	72,000 one-second records, approximately 20 h of instrumented passes selected for complete time stamps, cycle_id/segment_id linkage and pre/post comparability; dynamic plausibility checks only.
Weather/environment records	4392 segment-date records (366 days × 12 segments); rainfall, temperature and road wetness used as daily controls, not raw high-frequency weather-station data.
Maintenance and downtime events	389 service/downtime records from maintenance logs; used only for road-sensitive event-rate and mechanical-load-risk interpretation.
Data provenance	Anonymized industrial records provided by the site operator from dispatch/VIMS/maintenance-log systems; raw identifiers restricted by industrial confidentiality.

Table 1 reports only dataset volume, provenance and analytical role. the duplicated traceability rows were removed from Table 1 to reduce redundancy. Table 2 shows the grouping of intervention and control segments by route contours and close slope ranges. The initial conditions are not expected to coincide completely. Subsequent evaluation uses pre-trend diagnostics and fixed-effects adjustments.

Table 2. Haul-road segment passport, experimental role and route-matching structure.

Segment	Route	Length, m	Width, m	Mean Grade, %	Max Grade, %	Role	Repair Date
S001	R01	780	26	1.940	4.640	baseline	
S002	R01	920	28	5.790	6.980	baseline	
S003	R01	1180	26	6.150	8.700	intervention	15 August 2024
S004	R01	1120	30	5.820	7.050	control	
S005	R02	960	28	7.900	9.510	intervention	3 September 2024
S006	R02	1010	24	7.020	8.960	control	
S007	R03	1360	24	3.040	5.350	intervention	20 September 2024
S008	R03	1290	28	3.210	5.840	control	
S009	R03	880	24	6.180	7.760	intervention	6 October 2024
S010	R03	940	30	6.050	7.480	control	
S011	R04	1240	28	7.090	9.310	intervention	24 October 2024
S012	R04	1160	30	6.720	8.870	control	

Table 3 defines the matched-control calculation windows and the three-day washout interval. The resulting DiD sample contains 2634 cycle–focal-segment observations. The full register of 30,808 valid cycles is used for background characterization, whereas intervention coefficients are estimated only from the matched windows.

Table 3. Before–after matched-control windows used for DiD estimation.

ID	Intervention Segment	Control Segment	Repair Date	Washout Days	Before Event Window	After Event Window	n Before	n After	Control n Before	Control n After
INT001	S003	S004	15 August 2024	3	−21 to −1 days	+4 to +24 days	133	142	123	133
INT002	S005	S006	3 September 2024	3	−21 to −1 days	+4 to +24 days	130	129	125	142
INT003	S007	S008	20 September 2024	3	−21 to −1 days	+4 to +24 days	138	134	130	120
INT004	S009	S010	6 October 2024	3	−21 to −1 days	+4 to +24 days	140	126	127	136
INT005	S011	S012	24 October 2024	3	−21 to −1 days	+4 to +24 days	124	134	127	141
Total	5	5	—	3			665	665	632	672

Table 4 clarifies the status of each variable. Rolling-resistance descriptor and suspension-stress proxy are used for comparative interpretation of the repair effect but are not treated as direct force or strain gauge measurements.

Table 4. Measurement traceability and proxy-construction logic for the revised field study.

Variable/Outcome	Primary Source	Construction and Analytical Use	Main Limitation
Cycle–focal-segment observation	Dispatch/VIMS registry linked with segment_id and route_id	Nested unit used in DiD: cycle outcomes are linked to the focal segment traversed by the truck.	Not a randomized observation; repeated cycles are clustered by truck and segment.
Fuel for analyzed trips	Cycle-level fuel record from dispatch/VIMS fuel accounting	Used as L/cycle for trips traversing the focal segment and as route-normalized FI using full cycle distance Dcycle; not interpreted as fuel physically consumed only inside the repaired chainage.	Includes route, queue, idle and dispatch effects; controlled by matched design and covariates.
Cycle time for analyzed trips	Cycle start/end timestamps and dispatch records	Used as min/cycle for trips traversing the focal segment; interpreted cautiously because cycle time includes non-road delays.	Sensitive to loading, queueing and dispatching; conditional fit metrics are not interpreted as predictive accuracy.
Segment speed	GPS/VIMS segment-entry and segment-exit alignment	Local segment traversal speed, km/h, used as the most direct operational segment response.	May be affected by safety rules, traffic and operator behavior.
IRI and rut depth	Repeated UAV/LiDAR road-profile surveys	Profile filtered and aggregated by segment/date; used as independent road-state input.	Survey timing and surface moisture can affect local profile estimates.
Apparent rolling-resistance descriptor	Road-condition survey, profile descriptors, wetness and defect class	Used as segment-date road-severity descriptor and apparent CRR in physical interpretation.	Not a direct wheel-force or drawbar-pull measurement.
Vibration RMS	Telemetry/IMU-aligned records and cycle summaries	Used as local dynamic excitation indicator.	Depends on sensor mounting, speed and payload.
Suspension-stress proxy	Aligned telemetry/service variables: vibration RMS, vibration peak, payload, speed, IRI, rut depth and apparent RR descriptor.	MPa-eq. proxy calculated from a normalized mechanical-load index and service-calibrated proxy scale; used only for comparative before–after interpretation.	Not a strain-gauge measurement of structural stress; absolute MPa-eq. values are not used as component-level stress evidence.

The composition and sampling protocol of the limited 1 Hz telemetry subset are given in Table 5; this table shows which second records were used for dynamic validation.

Table 5. Composition and selection protocol of the 1 Hz telemetry subset.

Subset Component	Segments/Phase	Truck IDs (Anonymized)	Loaded State	Passes/Seconds	Selection Rationale
Representative repaired segment before	S003 before	T03, T07, T11	Loaded and return passes	18 passes/18,000 s	High-severity pre-maintenance profile with complete cycle linkage
Representative repaired segment after	S003 after washout	T03, T07, T11	Loaded and return passes	18 passes/18,000 s	Same focal segment after profile correction and washout interval
Matched-control comparison	S004 before/after windows	T02, T06, T09	Comparable duty state	18 passes/18,000 s	Background dynamic variability without road intervention
Additional validation traverses	S005/S006 and S007/S008 windows	T04, T08, T12	Mixed loaded/empty	18 passes/18,000 s	Check that telemetry pattern is not unique to S003
Total	Selected focal-segment traverses	9 anonymized trucks	Loaded/empty coded	72,000 one-second records	Dynamic plausibility subset; not a full-year 1 Hz fleet stream

Table 5 shows the composition of a limited second subarray: this is not the full annual 1 Hz data stream for 12 trucks but selected instrumented passes through repaired and matched-control sections. The subarray is used to analyze the physical form of the effect at the velocity, vibration, and mechanical-load proxy.

3.7. Comparability, Pre-Trends and Uncertainty

Since the areas to be repaired were deliberately selected as more degraded, full equality of intervention and control levels was not assumed before the repair. Therefore, comparability was assessed not by the absolute coincidence of the initial values, but by three criteria: the proximity of the route-geometric role, the absence of a statistically significant divergence of pre-repair trends, and the stability of the effect after regression adjustment.

Pre-trends were checked in the event-time coordinate with reference to the date of the intervention. In addition, cluster-robust and wild-bootstrap intervals for key DiD effects were evaluated. This approach is needed to take into account the dependence of cycles within segment pairs, the repeatability of observations on the same dump trucks, and a limited number of intervention segments.

3.8. Engineering Interpretation, Prioritization and Application Limits

Engineering prioritization was carried out based on the results of a quasi-experimental assessment. The segment received high priority with a combination of fine traffic indicators, confirmed operational response and mechanical loading. Ranking translates the results of the DiD into a sequence of road works and is not a separate predictive model.

The application boundary was set as follows: the obtained coefficients can be used to plan maintenance within a similar site, class of dump trucks and road material, but cannot be mechanically transferred to other quarries without local calibration. The decision to repair should also take into account the cost of intervention, the availability of equipment, the impact on the production schedule, seasonality and the risk of re-degradation of the pavement.

3.9. Reproducibility, Assumptions and Limits of Interpretation

The calculation base was organized according to independent contours: cycle registry, segment passport, intervention–control design, UAV/LiDAR profile, road-condition surveys, fleet status, 1 Hz telemetry subset, weather/environment records, maintenance events and data-quality log. This organization allows you to repeat calculations from the level of an individual cycle and road profile to aggregated DiD estimates.

The interpretation of the results is limited by the quasi-experimental nature of the design. The repaired and control segments were compared according to the observed signs and checked against pre-repair trends, but full randomization of road interventions in the existing quarry is not possible. Therefore, the conclusion is formulated as a field-supported intervention effect under matched-control and pre-trend assumptions, rather than as laboratory-isolated causality.

An additional limitation is related to the portability of the results. The obtained coefficients should not be mechanically transferred to other quarries, classes of dump trucks, climatic seasons or types of pavement without local calibration. At the same time, the methodological scheme—independent road profiling, cycle-register, matched-control DiD, pre-trends, uncertainty intervals and 1 Hz dynamic check—is suitable for repetition in subsequent industrial studies.

4. Results

4.1. Physical Improvement of the Road Condition After the Intervention

In the first step, it was evaluated whether the road intervention led to a measurable change in the independent parameters of the road condition. First, the profile, rutting and apparent rolling-resistance descriptor were analyzed, then the operational and mechanical responses. Figure 5 maps the intervention and control segments before and after the intervention against the main road metrics.

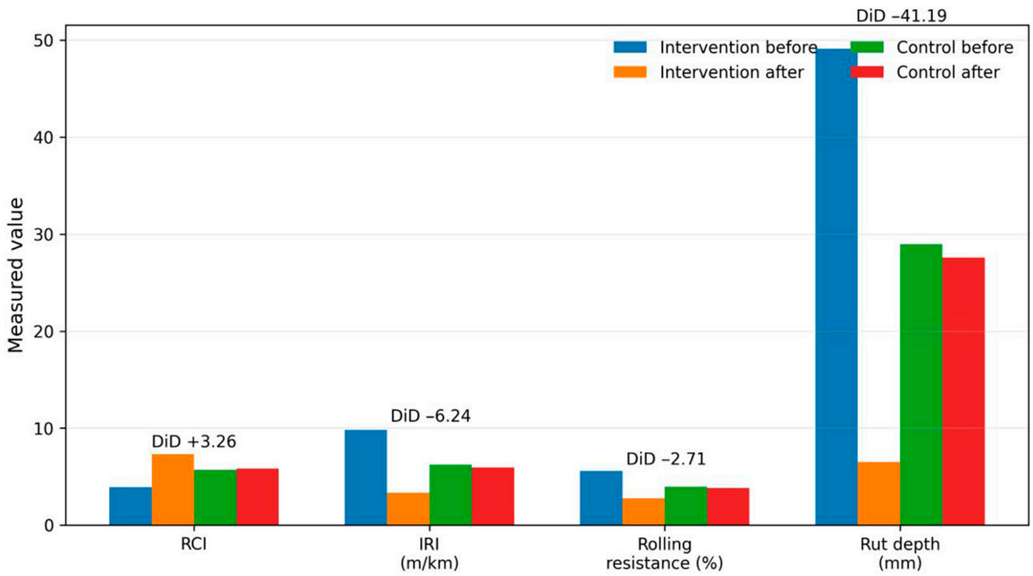

Figure 5. Road-condition response after haul-road maintenance in intervention and matched-control segments.

Figure 5 shows that on the repaired segments, the change in road condition has a pronounced directional character: RCI increases, and IRI, rolling resistance and rut depth decrease. At the control segments, the changes remain small, so the subsequent DiD assessment separates the repair shift from the background calendar variability. A quantitative assessment of the change in road parameters is presented in Table 6. The table stores the before/after levels for the intervention and control groups, which allows you to see both the final difference-in-differences and the initial asymmetry of the segments.

Table 6. Difference-in-differences road-condition effects after haul-road maintenance.

Metric	Intervention Before	Intervention After	Delta Intervention	Control Before	Control After	Delta Control	DiD Effect
RCI	3.93	7.31	+3.38	5.69	5.81	+0.12	+3.26
IRI, m/km	9.82	3.33	−6.49	6.22	5.97	−0.25	−6.24
Apparent rolling-resistance descriptor, %	5.60	2.78	−2.82	3.97	3.85	−0.12	−2.71
Rut depth, mm	49.1	6.5	−42.6	29.0	27.6	−1.4	−41.2

Table 6 confirms that the intervention segments did not receive a cosmetic, but a physically measurable improvement in road condition. The most pronounced shift is obtained by IRI and rut depth, i.e., by parameters directly related to the vertical excitation of the machine and additional loss of motion.

4.2. Operational and Mechanical Response of the Transport Cycle

After confirming the change in the road environment, the analysis was moved to the "cycle-focus segment" observation level. The main responses are fuel consumption per cycle for trips through the analyzed section, route-normalized fuel intensity over the full length of the trip, the corresponding cycle time, segment speed, RMS vibration and suspension-stress proxy. Figure 6 shows the direction of change in these indicators after repair.

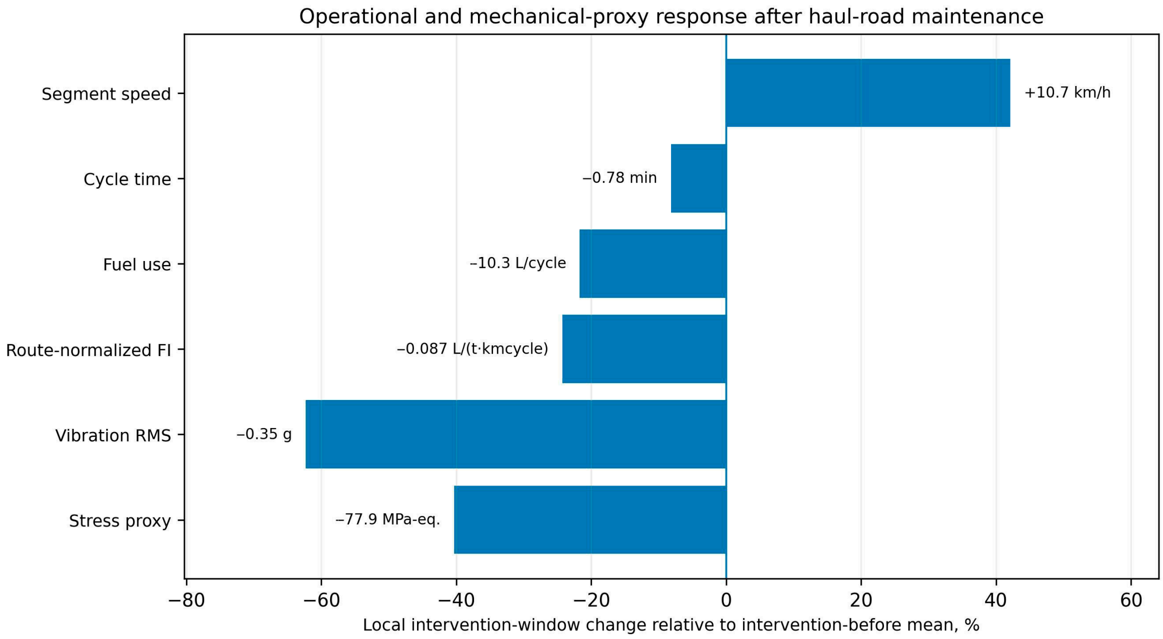

Figure 6. Operational and mechanical-proxy response after haul-road maintenance; raw DiD effects are shown next to local intervention-window percentage changes.

The scale of the result must be considered before interpreting Figure 6. The intervention segments were selected as areas with a pronounced initial degradation of the profile, so large unidirectional changes belong to the local intervention-window and are not transferred to the entire road network.

Figure 6 shows a coherent multichannel response. Relative to the intervention-before mean, fuel use decreased by approximately 22%, cycle time by 8.2%, vibration RMS by about 62%, and the suspension-stress proxy by about 40%, while segment speed increased by approximately 42%. These percentages describe the selected high-severity intervention window and are not annual fleet-average coefficients.

The full numerical form of the operational and mechanical effects is given in Table 7. Here, the absolute values of the indicators before and after the intervention are stored in order to separate, in fact, the DiD effect from the differences in the initial level between the intervention and control segments.

Table 7. Difference-in-differences operational and mechanical-proxy effects for analyzed trips traversing focal segments.

Metric	Intervention Before	Intervention After	Delta Intervention	Control Before	Control After	Delta Control	DiD Effect
Segment speed, km/h	25.4	36.8	+11.4	33.3	34.1	+0.8	+10.7
Cycle time for analyzed trips, min	9.46	8.54	−0.92	8.84	8.70	−0.14	−0.78
Fuel for analyzed trips, L/cycle	47.2	36.5	−10.8	35.3	34.8	−0.5	−10.3
Route-normalized fuel intensity, L/(t·kmcycle)	0.358	0.269	−0.089	0.265	0.262	−0.002	−0.087
Vibration RMS, g	0.562	0.199	−0.363	0.370	0.357	−0.013	−0.350
Suspension-stress proxy, MPa-eq.	193.1	112.2	−80.9	151.7	148.6	−3.0	−77.9

Table 7 shows that the largest relative changes are obtained from mechanical response: vibration and suspension-stress proxy. For selected high-severity road segments, this is consistent with the effect of local roughness and rutting on the shock and cycling load of the undercarriage. The absolute values of DiD effects refer to local intervention-window estimates.

The distribution variability of the main indicators is shown separately in Table 8. The table shows that the average effects are formed against the background of intra-group variance related to payload, speed, humidity, queues, operator mode and differences between dump trucks.

Table 8. Distributional variability of main outcomes in the local DiD window.

Outcome	Intervention Before, Mean ± SD	Intervention After, Mean ± SD	Control Before, Mean ± SD	Control After, Mean ± SD	Typical IQR in DiD Window
Fuel for analyzed trips, L/cycle	47.2 ± 7.8	36.5 ± 6.2	35.3 ± 5.9	34.8 ± 5.7	31.2–43.9
Cycle time, min	9.46 ± 1.35	8.54 ± 1.18	8.84 ± 1.21	8.70 ± 1.16	7.8–9.9
Segment speed, km/h	25.4 ± 5.6	36.8 ± 6.4	33.3 ± 5.8	34.1 ± 5.9	29.4–38.7
Vibration RMS, g	0.562 ± 0.146	0.199 ± 0.071	0.370 ± 0.103	0.357 ± 0.098	0.22–0.48
Suspension-stress proxy, MPa-eq.	193.1 ± 34.8	112.2 ± 24.5	151.7 ± 29.6	148.6 ± 28.9	118–176

Table 8 shows that the effect of repair is not perfectly the same for all observations. SD and IQR values preserve industrial variability related to payload, speed, humidity, queues, operator mode, and differences between trucks.

4.3. Regression Adjustment, Uncertainty and Engineering Significance

To avoid treating the results as a simple comparison of averages, DiD effects were re-evaluated in the regression specification with production covariates, fixed effects of the segment and dump truck, and cluster/bootstrap-oriented uncertainty estimation. Figure 7 shows the ratios and 95% confidence intervals for the main responses.

Figure 7 shows that the 95% intervals remain on the expected side of zero for all primary responses. The fuel coefficient is −10.6 L/cycle (95% CI: −12.5 to −9.0), cycle time is −0.78 min (−1.51 to −0.14), segment speed is +10.7 km/h (+8.2 to +12.9), vibration RMS is −0.351 g (−0.414 to −0.296), and the suspension-stress proxy is −78.2 MPa-eq. (−91.6 to −64.8). The split horizontal scale prevents the much larger stress-proxy coefficient from compressing the remaining intervals.

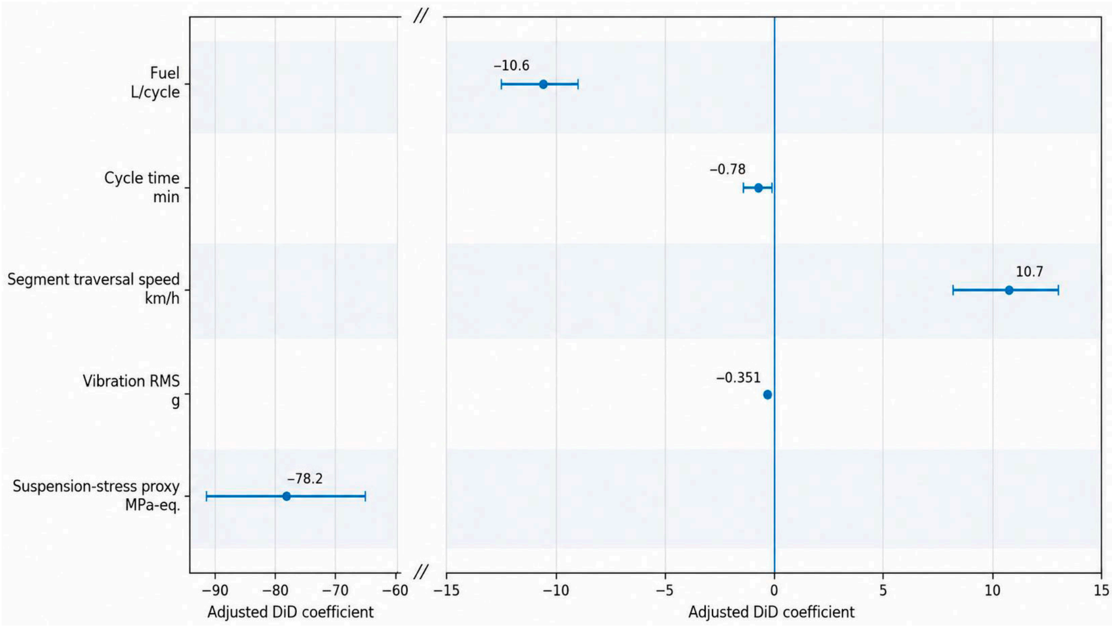

Figure 7. Regression-adjusted DiD effects with cluster/wild-bootstrap 95% confidence intervals for the local DiD window.

Table 9 confirms that the direction and magnitude of the local fuel, speed, vibration and stress-proxy effects remain stable after adjustment for production covariates and fixed effects. Cycle time has the widest relative interval because it also depends on queues, loading and dispatching; this uncertainty is carried into the engineering interpretation rather than treated as predictive-model error.

Table 9. Regression-adjusted DiD estimates with uncertainty intervals for local intervention-window effects.

Outcome	Adjusted Local DiD Coefficient	95% CI	*p*-Value	Inference Basis	n
Fuel for analyzed trips, L/cycle	−10.6	−12.5 to −9.0	<0.01	Segment/truck/event-period FE; cluster/WB CI	2634
Cycle time for analyzed trips, min	−0.78	−1.51 to −0.14	0.018	Segment/truck/event-period FE; cluster/WB CI	2634
Segment traversal speed, km/h	+10.7	+8.2 to +12.9	<0.01	Segment/truck/event-period FE; cluster/WB CI	2634
Vibration RMS, g	−0.351	−0.414 to −0.296	<0.01	Segment/truck/event-period FE; cluster/WB CI	2634
Suspension-stress proxy, MPa-eq.	−78.2	−91.6 to −64.8	<0.01	Segment/truck/event-period FE; cluster/WB CI	2634

Statistical and engineering significance were evaluated separately. The 0.78 min reduction is 8.2% of the 9.46 min intervention-before mean; at the base scenario of 3650 comparable cycles/year, it corresponds to approximately 47.5 truck-hours/year. The adjusted fuel reduction of 10.6 L/cycle is 22.5% of the 47.2 L/cycle intervention-before mean and corresponds to about 38,700 L/year under the same scenario. These annualized values are scenario consequences, not additional causal estimates, but they demonstrate that a statistically significant coefficient also has an operationally material scale.

4.4. Segment Comparability, Event-Time and Robustness Checks

Since the areas to be repaired were selected as more problematic, full equality of the intervention and control segments before the intervention is not a realistic requirement. A more important condition for DiD interpretation is that there are no different pre-trends before the repair date. A diagnostic comparability table is provided in Table 10.

Table 10. Pre-intervention contrast and event-trend diagnostics for intervention and matched-control segment pairs.

Pair	Route	n Int./Ctrl.	Payload Diff, t	IRI Gap, m/km	Fuel Gap, L/Cycle	Pre-Trend *p*/Slope Diff
S003-S004	R01/R01	133/123	−1.2	+3.60	+11.1	0.74/+0.03 L/cycle/day
S005-S006	R02/R02	130/125	−3.9	+3.24	+2.6	0.68/−0.02 L/cycle/day
S007-S008	R03/R03	138/130	−0.5	+2.87	+6.8	0.59/+0.04 L/cycle/day
S009-S010	R03/R03	140/127	+0.9	+3.37	+5.2	0.71/+0.01 L/cycle/day
S011-S012	R04/R04	124/127	+2.1	+3.08	+4.1	0.64/−0.03 L/cycle/day

Table 10 reports baseline contrasts and pre-intervention trend diagnostics. Repaired segments were deliberately more degraded, so level equality was neither expected nor claimed. The pair-level pre-trend p-values of 0.59–0.74 indicate no detectable divergence within the available pre-window, although they cannot prove equality of unobserved counterfactual trajectories.

The 14-day lead-placebo/event-time diagnostic did not identify a systematic pseudo-intervention effect: all pair-level pre-period trend contrasts remained non-significant (p = 0.59–0.74). The non-negative cohort-weighted group-time ATT was −10.60 L/cycle for fuel, +10.73 km/h for speed and −77.96 MPa-eq. for the suspension-stress proxy, closely matching the corresponding TWFE estimates of −10.6, +10.7 and −78.2. Thus, the reported average is not driven by a negative-weight comparison among differently timed treatment cohorts.

Event-time dynamics indicate when there is a gap between intervention and control trajectories. Figure 8 compares fuel consumption, IRI, and suspension-stress proxy relative to the repair date. The interval of 0–3 days is shown as the washout period.

Figure 8 shows that prior to the intervention date, the intervention and control segments differed in level but did not show divergent pre-trends. After the washout period is over, the intervention paths change in concert with the physical improvement of the road: IRI, fuel consumption, and suspension-stress proxy decrease, while control segments maintain background dynamics.

4.5. Heterogeneity of the Effect on the Repaired Segments

Segment-specific DiD effects were calculated to assess the heterogeneity of the effect. Such testing is important when the number of intervention segments is small, since the average effect may depend on individual sites. Figure 9 visualizes the heterogeneity of fuel and mechanical response.

Figure 9 shows heterogeneous magnitudes but a common effect direction across all five repaired segments. Fuel effects range from −9.0 to −13.1 L/cycle and stress-proxy effects from −75.2 to −80.0 MPa-eq.; therefore, the pooled result is not generated by a single extreme repair. The remaining variation is consistent with differences in initial IRI, geometry, traffic intensity and repair execution.

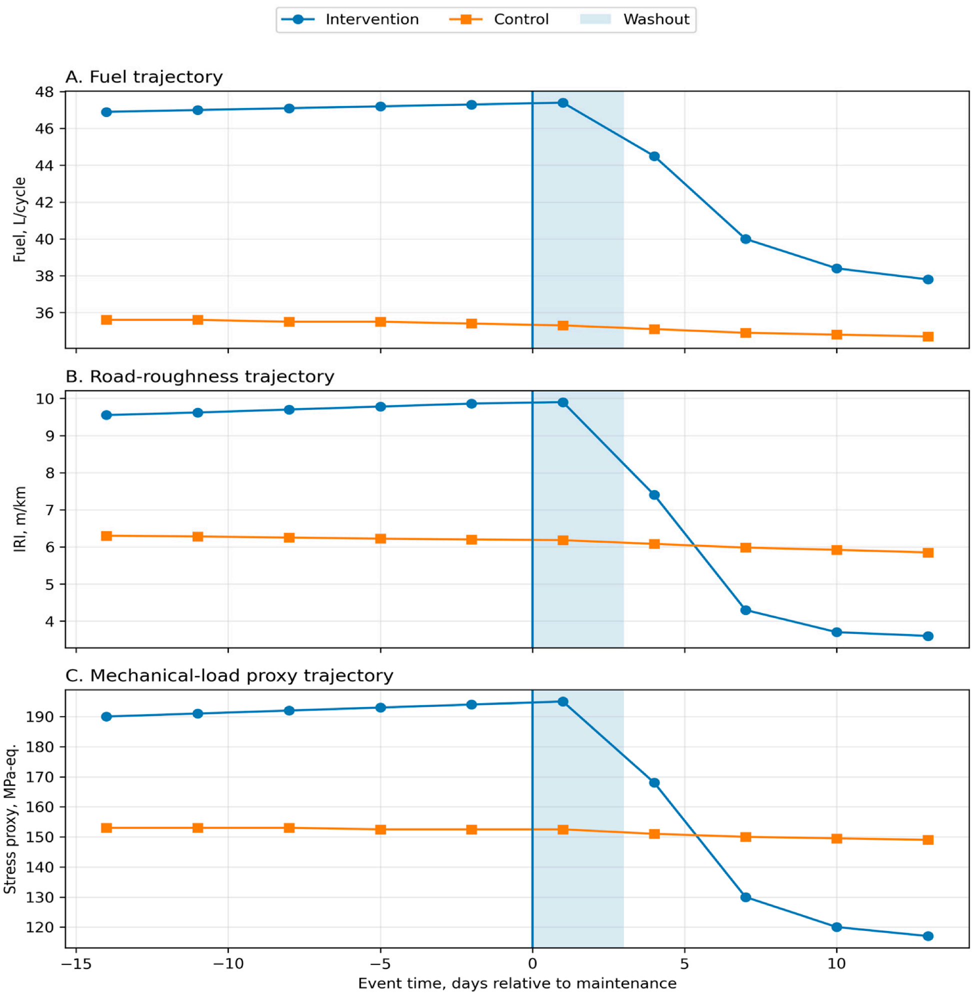

Figure 8. Event-time trends for fuel consumption, IRI and suspension-stress proxy before and after haul-road intervention.

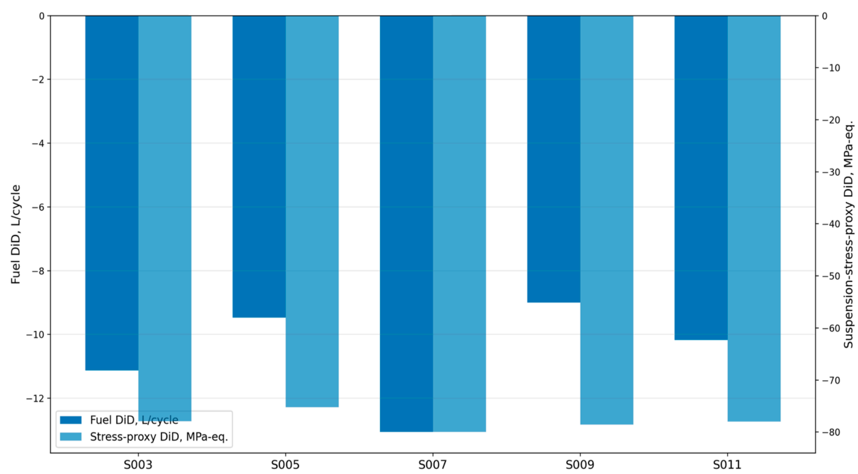

Figure 9. Segment-level heterogeneity of fuel and suspension-stress-proxy DiD effects across repaired road segments.

Table 11 shows the repeatability of the effect sign across all repaired segments. The differences between segments reflect operational heterogeneity related to the original IRI, geometry, traffic, and type of recovery performed.

Table 11. Segment-specific DiD effects for repaired haul-road segments.

Segment	Control	n Before/After	IRI Before→After	Fuel DiD, L/Cycle	Speed DiD, km/h	Stress-Proxy DiD, MPa-eq.
S003	S004	133/142	9.9→3.4	−11.1 [−13.4; −8.9]	+10.5	−77.9 [−91.8; −64.0]
S005	S006	130/129	9.6→3.2	−9.5 [−11.7; −7.1]	+10.6	−75.2 [−88.4; −62.2]
S007	S008	138/134	8.9→3.5	−13.1 [−15.8; −10.2]	+11.2	−80.0 [−94.0; −66.1]
S009	S010	140/126	10.1→3.1	−9.0 [−11.3; −6.7]	+11.2	−78.6 [−92.1; −65.1]
S011	S012	124/134	9.7→3.4	−10.2 [−12.6; −7.8]	+10.1	−78.0 [−91.7; −64.4]

4.6. Dynamic Confirmation by 1 Hz Telemetry

The 1 Hz telemetry subset is a dynamic subarray for the analysis of the traversal of the restored section. Its volume is 72,000 s recordings, or approximately 20 h of instrumented passes, selected for completeness, temporality, segment_id/cycle_id consistency and the presence of pre- and post-repair observations. This layer is separate from the cycle-level register and is not used as an annual second telemetry stream.

The dynamic form of the local effect at the second level is shown in Figure 10; the graph compares the speed, vibration RMS, and suspension-stress proxy along the repaired segment S003 before and after the repair.

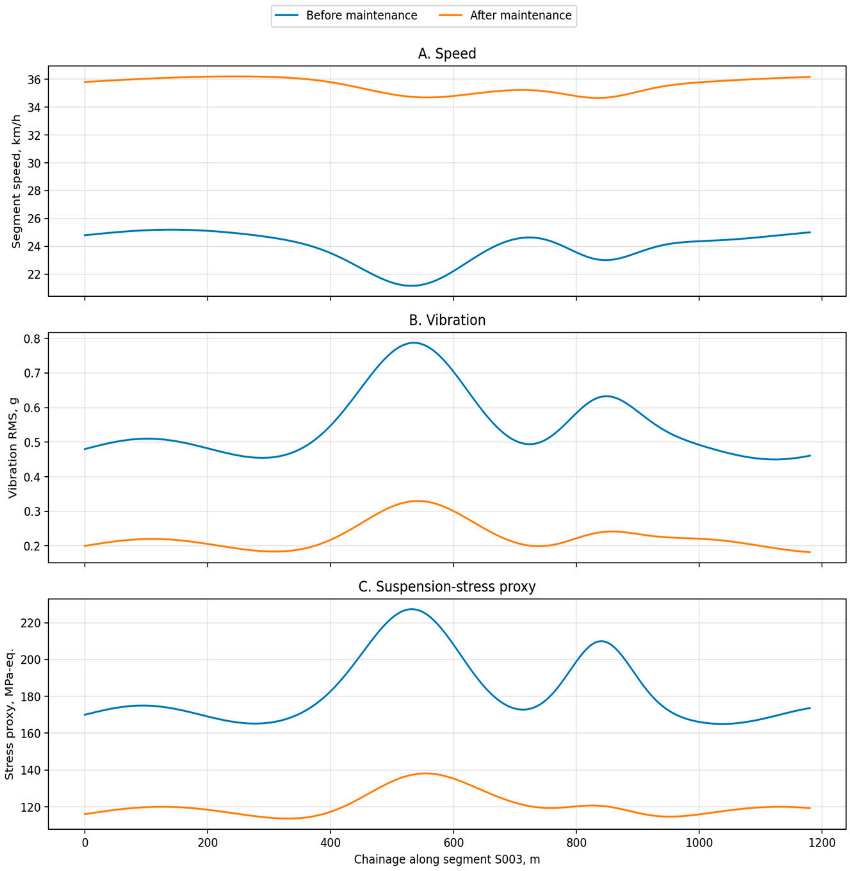

Figure 10. Representative 1 Hz telemetry-subset response along repaired segment S003 before and after maintenance.

Figure 10 localizes the dynamic response along segment S003. Before maintenance, the principal vibration and stress-proxy peaks occur near chainage 500–600 m and 800–900 m; after maintenance, these peaks are substantially attenuated while speed becomes higher and more uniform. The figure therefore supports the mechanism of roughness-induced dynamic loading rather than merely repeating the cycle-level mean comparison.

Summary telemetry-derived metrics are given in Table 12. They are not used to replace DiD estimation, but they confirm that a decrease in average cycle-level effects is also observed in the dynamics of the car's movement.

Table 12. Representative 1 Hz telemetry indicators before and after maintenance on segment S003.

Telemetry Indicator	Before Maintenance	After Maintenance	Engineering Interpretation
S003 mean segment speed along repaired window	24.8 km/h	35.9 km/h	Higher and more stable speed after road-profile correction
95th percentile vibration	0.78 g	0.31 g	Lower high-frequency excitation on repaired chainage
Stress proxy MPa-eq.	218 MPa-eq.	136 MPa-eq.	Lower mechanical peak burden after maintenance
Braking events per km	0.86	0.41	Reduced forced braking on rough-profile zones
Gear shifts per km	1.70	1.02	Smoother traction regime after maintenance

Table 12 confirms that the improvement of the road is not only reflected in the average per cycle, but also in the driving pattern: sharp mechanical peaks, braking and gear shifts are reduced. This strengthens the physical interpretation of the quasi-experimental DiD estimate, but does not extend the calculated effect window beyond the matched-control sample.

4.7. Mechanical Loading, Short-Term Maintenance Events, and Engineering Sensitivity

The reliability block is limited to the reliability-related mechanical-load-risk score. A consistent reduction in vibration RMS, suspension-stress proxy, road-sensitive maintenance-event intensity, and mechanical-load proxy is shown. A separate seasonal array of component-level events is required to infer the hazard rate, MTBF, or long-term probability of failure.

Before you can interpret the road-sensitive maintenance-event rate, you must determine which maintenance records were considered road-sensitive. This classification is given in Table 13 and separates mechanical-load-related events from planned maintenance and non-road failures.

Table 13. Definition of road-sensitive maintenance-event categories used in the short-window reliability-related analysis.

Category	Included Examples	Reason for Inclusion/Exclusion
Included tire events	Tire cuts, sidewall damage, abnormal tread damage after rough-road operation	Directly sensitive to rutting, potholes, sharp edges and rough rolling conditions.
Included suspension events	Suspension cylinder inspection, strut/shock absorber service, abnormal suspension-pressure check	Mechanically related to vertical excitation and repeated impact loads.
Included frame/chassis inspections	Post-vibration inspection, abnormal chassis noise, repeated mechanical-load alarms	Used only as road-sensitive service context, not as confirmed structural failure.
Included brake/gear-shift-related checks	Inspection after frequent braking or gear-shift anomalies on rough segments	Linked to forced speed changes on degraded road sections.
Excluded scheduled maintenance	Calendar-based service, planned oil/filter replacement, routine inspections	Not attributable to road condition within the short DiD window.
Excluded non-road causes	Engine faults, electrical faults, operator absence, loader delay, dispatching delays	May affect cycle time or downtime but do not represent road-sensitive mechanical loading.

Road-sensitive maintenance events were coded according to predefined engineering rules based on maintenance-log descriptions. Events were included only when the service description referred to tires, suspension, chassis/frame inspection, vibration alarm or rough-road damage context; scheduled maintenance, engine/electrical failures, operator absence and loading-equipment delays were excluded. Ambiguous records were not used for the road-sensitive event-rate comparison. The resulting included and excluded event categories are summarized in Table 13.

Table 13 makes the reliability-related block reproducible: maintenance events are not used as full-fledged failure statistics, but serve as a short-term indicator of the road-dependent mechanical load. A summary of the intensity of road-sensitive events, downtime intensity, and mechanical-load proxy by intervention/control phases is given in Table 14.

Table 14. Road-sensitive maintenance-event rates and mechanical-load proxy across experimental phases.

Group	Valid Segment-Linked Cycles	Road-Sensitive Events	Events/1000 Cycles	Downtime h/1000 Cycles	Mechanical-Load Proxy
Intervention before	665	34	51.13	65.0	2.149
Intervention after	665	18	27.07	30.5	0.429
Control before	632	26	41.14	48.0	1.049
Control after	672	25	37.20	45.5	0.988

Table 14 shows a short-window reduction in road-sensitive event rate, downtime intensity and mechanical-load proxy after repair. These quantities are supporting engineering indicators only. They do not establish a lower component hazard rate, longer MTBF or reduced lifetime failure probability; those claims require a longer component-resolved dataset with censoring and survival analysis.

After statistical and mechanical verification, the effects are translated into a maintenance-priority visualization. In Figure 11A, the horizontal axis is local fuel-saving potential (the magnitude of the segment-specific fuel DiD effect, L/cycle), and the vertical axis is local mechanical-load-reduction potential (the magnitude of the segment-specific suspension-stress-proxy DiD effect, MPa-eq.). Each labeled point represents one monitored road segment. Intervention and control markers are shown separately, and the shaded zones are site-specific screening bands rather than statistical-significance thresholds. Figure 11B ranks the same segments by the composite $Priority_i$ score.

Figure 11 shows why these two dimensions were selected: fuel saving represents the direct operating-cost channel, whereas stress-proxy reduction represents the mechanical-load channel. Intervention segments occupy the high-priority zone because both penalties are large; control segments remain in the monitoring zone. The right-hand ranking does not create new evidence but summarizes the same measured dimensions together with the predefined time and road-severity components. Table 15 then converts the fuel and time effects into scenario-based economic sensitivity.

Table 15 shows that positive net benefit persists in all three scenarios, but the magnitude of the economic result depends on the intensity of trips, the price of fuel, the cost of an hour of dump truck, the length of the section to be repaired and the actual cost of road rehabilitation. Therefore, the economic conclusion is considered as engineering sensitivity, and not as a universal payback standard.

The Section 4 section integrates independent road improvement measurement, DiD assessment of operational and mechanical response, uncertainty checking, event-time diagnostics, segmental reproducibility, telemetry confirmation, short-term road-sensitive events, and engineering interpretation. Service prioritization is given after assessing the effect of road intervention.

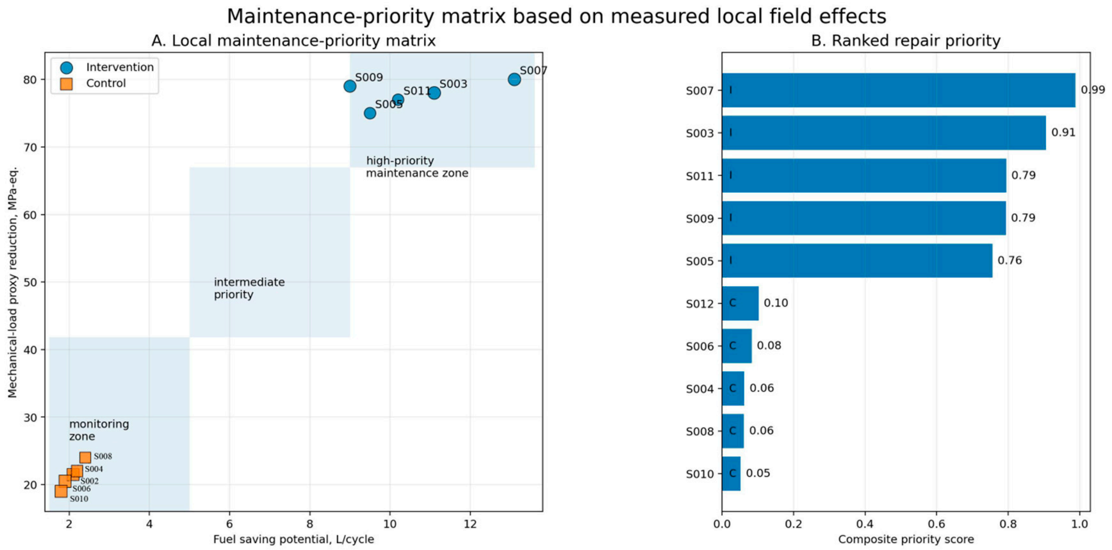

Figure 11. Maintenance-priority matrix and ranked repair-priority score based on measured local fuel and mechanical-load effects of road segments. In Panel (**B**), "I" indicates road segments assigned to the intervention group, whereas "C" denotes road segments belonging to the control group.

Table 15. Economic sensitivity and payback scenarios based on measured local DiD effects.

Scenario	Cycles/Year Through Comparable Segments	Diesel USD/L	Truck USD/h	Gross Benefit	Road Cost Assumption	Net Benefit	Payback
Conservative	3000	0.92	254	38.2k USD/year	12.5k USD [10–15k]	25.7k USD/year	about 120 days
Base	3650	1.08	318	55.5k USD/year	7.8k USD [6.2–9.8k]	47.7k USD/year	about 50 days
Intensive	4500	1.24	382	79.6k USD/year	11.0k USD [8.8–13.5k]	68.6k USD/year	about 50 days

5. Discussion

5.1. Physical Mechanism of Road Influence on Fuel, Cycle Time and Mechanical Loading

The concept of the article shifts the discussion from the general formula "the condition of the road affects energy efficiency and reliability" to a more testable field hypothesis: the repair of the technological segment should simultaneously improve independent road performance and reduce the operational and mechanical penalty of the transport cycle.

Physically, this result is explained not by a single factor, but by a combination of several mechanisms. A decrease in the apparent rolling-resistance descriptor is consistent with a decrease in the portion of tractive effort associated with road resistance. Reduced IRI and rutting stabilizes travel speed, reduces forced braking and re-acceleration, and reduces shock vertical and transverse suspension excitation. Therefore, the mechanical proxy response is stronger than the fuel response: vibration RMS and suspension-stress proxy are sensitive to local defects, while fuel additionally depends on payload, grade, idle time, bursts and engine mode.

The higher residual variability of cycle time requires special explanation. It does not contradict the road effect, but shows that the duration of the trip is a mixed production-organizational variable. It is formed not only by road resistance and permissible speed, but also by waiting time, loading mode, oncoming traffic, dispatch restrictions and local safety rules. Therefore, it is more correct to interpret the sign and stability of the DiD coefficient for cycle time, rather than expecting the same high explanation as for vibration RMS or suspension-stress proxy.

5.2. Why a Quasi-Experimental Framework Is Stronger than Simple Predictive Logic

A regression or predictive model shows a statistical relationship between road conditions and fuel consumption, but does not separate the effect of road intervention from background variability caused by weather, shifts, queues, loading, truck individualities, and calendar changes in the pit regime. In this study, road repair is considered as an observable field event, and predictive and economic analytics are performed after assessing the intervention effect.

Compared to the simple regression "bad road—high fuel consumption", quasi-experimental staging uses road intervention as an observable field event. Intervention segments are mapped to control segments, and the effect is evaluated as a difference in change, not as a difference in levels. Therefore, the results give a field-supported interpretation under matched-control, pre-trend and fixed-effects assumptions without asserting laboratory-isolated causality. The final interpretation logic is shown in Figure 12. The diagram separates the measurement base, statistical evaluation, dynamic confirmation, the boundary of reliable interpretation, and the engineering application of the results.

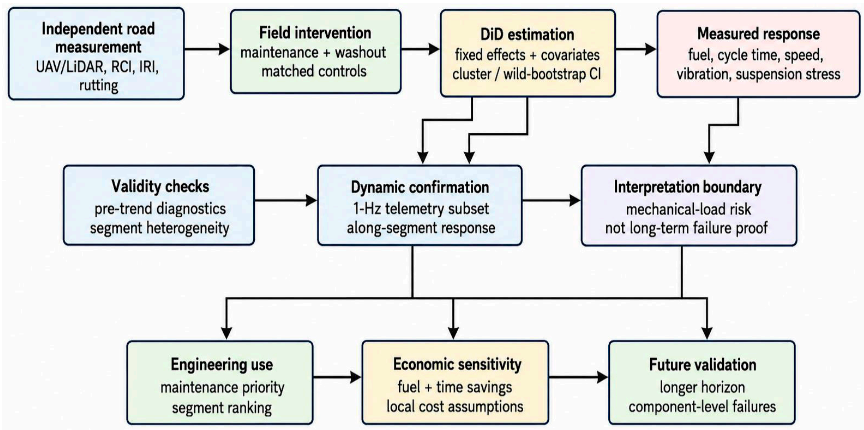

Figure 12. Evidence hierarchy and interpretation boundary linking road measurement, field intervention, DiD estimation, telemetry confirmation and engineering use.

Figure 12 shows the interpretation boundary: the main results relate to measured fuel, time and mechanical responses, rather than total long-term fleet failure. The maintenance-priority matrix and economic sensitivity follow the DiD results.

5.3. Mechanical-Load Risk Instead of Direct Proof of Reliability

The limitation on reliable interpretation is due to a short before–after window. To fully infer long-term failure, component-level failure logs, event classification by nodes, censorship accounting, seasonal recurrence, and survival/hazard analysis are required. The work on reliability analysis of mining trucks also emphasizes the need to consider failure at the level of components and subsystems, rather than replacing it with short-term diagnostic indicators [44].

Therefore, the reliability interpretation is limited by the reliability-related mechanical-load-risk reduction formula. This formulation is scientifically correct: it shows a decrease in vibration RMS, suspension-stress proxy, mechanical-load proxy, road-sensitive event rate, and downtime intensity, but does not claim a long-term reduction in failure without component-level survival/hazard evidence. For quarry fleet systems, similar logic is used in the availability- and reliability-oriented models of haul-truck fleets and open-pit fleet allocation [45,46].

In practice, this does not weaken the article. In contrast, a focus on mechanical loading makes the result more measurable in engineering. A road defect is seen as a manageable source of cyclic and shock loading, and road repairs are seen as a way to reduce the mechanical load before it shows up in failure statistics. For mining dump trucks, such a cautious boundary is especially important, since maintenance and repair operations include not only the technical condition of components, but also human, organizational and diagnostic factors [47].

5.4. The Role of UAV/LiDAR and 1 Hz Telemetry in the New Version of the Article

UAV/LiDAR is used as an independent road-measurement layer. IRI, rut depth and the apparent rolling-resistance descriptor are obtained before truck outcomes are statistically assessed, which preserves the exposure–outcome ordering. The 1 Hz subset then tests whether the estimated cycle-level effect has a physically plausible chainage-resolved form. Reference [48] used the same monitoring context for association analysis; the present study advances from association to an intervention-focused matched-control design.

Recent DiD literature emphasizes that staggered timing and heterogeneous treatment effects can contaminate conventional TWFE event-study coefficients. The added lead-placebo and cohort-weighted group-time ATT checks follow these methodological recommendations and are reported as robustness comparisons rather than as replacements for the primary matched-pair estimate [49,50].

1 Hz telemetry supplements the cycle-level register with a dynamic check of the rehabilitated section. This layer does not increase the statistical denominator of the DiD analysis, but shows the trajectory of speed, vibration, and mechanical-load proxy along the chainage. In this study, it is limited to about 20 h of instrumented passes.

5.5. Threats to Validity and Ways to Reduce Them

Because the study is performed in an active quarry, it cannot have the design of a fully randomized experiment. The areas to be repaired were originally selected as problematic, so the intervention and control groups should not be described as completely identical. A more correct formulation is that control segments are used to estimate background temporal dynamics, and initial level differences are taken into account through contrast diagnostics, fixed effects, operational covariates, and pre-trend checking [38,41,43].

The main threats to validity and the controls applied are summarized in Table 16. The table sets the limits of interpretation of the quasi-experimental design.

Table 16 summarizes the main limitations of interpretation and control measures. The table shows which prerequisites support field-supported quasi-experimental interpretation and which elements require subsequent industrial verification.

Table 16. Main threats to validity and mitigation logic for the revised quasi-experimental interpretation.

Threat to Validity	Why It Matters	Mitigation in the Revised Manuscript
Non-random intervention assignment	Road segments were repaired because they were degraded	Do not claim randomized causality; use matched-control DiD, pre-trend diagnostics and cautious quasi-experimental wording
Baseline imbalance	Intervention segments had worse initial IRI and fuel levels	Report before-period contrasts; interpret controls as background-dynamics references rather than identical twins
Repeated cycles within segment/truck	Cycle records are not fully independent	Use segment, truck and event-period fixed effects; estimate only Treat $\times$ Post under segment FE; apply cluster/wild-bootstrap uncertainty intervals.
Weather and operational variability	Rain, moisture, queues, payload and dispatching may confound cycle outcomes	Include operational covariates; separate road-condition effects from queue/idle-dependent cycle-time variability

Table 16. *Cont.*

Threat to Validity	Why It Matters	Mitigation in the Revised Manuscript
Short reliability horizon	Maintenance events do not yet prove long-term failure-rate reduction	Use mechanical-load-risk wording; require future component-level survival/hazard validation
Telemetry subset incompleteness	1 Hz records are representative, not complete for all valid cycles	Define telemetry as dynamic validation subset rather than the main statistical denominator
Single-site transferability	One mine, one truck class and a limited number of repaired segments	Present coefficients as site-specific; transfer method, not numeric constants, to other mines

5.6. Engineering Implications and Portability

The practical contribution of the article consists in the transition from visual and calendar maintenance of technological roads to maintenance based on a measurable fuel, time and mechanical penalty. If a segment simultaneously has a high IRI, rolling resistance, fuel penalty, suspension-stress penalty and a significant flow of trips, its repair has a double effect: it reduces the current energy and time losses and reduces the mechanical-load burden for the chassis of the dump truck.

At the same time, numerical coefficients should not be mechanically transferred to other quarries. They depend on the model of the dump truck, the weight of the cargo, the road material, the climate, the organization of traffic, the slopes, the repair mode and the quality of the initial telemetry. It is not the magnitude of the effect that is transferred, but the methodological scheme: independent road profiling, intervention–control pairing, event-time diagnostics, regression-adjusted DiD, telemetry confirmation and conservative engineering sensitivity.

Further work should expand the number of mines, truck classes, seasons and pavement materials; establish component-resolved reliability logs for tires, suspension, frame and brakes; and evaluate intervention durability beyond the short matched windows. A second development path is an integrated mine digital twin in which haul-road geometry, truck telemetry, AI-based anomaly detection and maintenance decisions are updated jointly. Microseismic monitoring can be incorporated as a complementary geotechnical-hazard layer for rock-mass instability and dynamic-disaster warning, but it should remain analytically distinct from the road-maintenance pathway because it measures internal fracture evolution rather than truck–road interaction [51,52].

6. Conclusions

This study demonstrates a quasi-experimental framework for evaluating haul-road maintenance as an observable field intervention. Its methodological contribution is the explicit separation of independent road measurement, cycle-level effect estimation, chainage-resolved telemetry confirmation and bounded engineering interpretation.

1. A multi-source industrial array of the open-pit transport system has been formed, but its analytical layers are separated by purpose: 30,808 valid cycle-level records are used for background characterization and verification of physical dependencies, while the main effect of the repair is estimated only in matched-control DiD windows with a volume of 2634 "cycle-focus segment" observations.

2. Repair and profiling activities in five intervention segments led to a measurable physical improvement in road condition: RCI increased, while IRI, apparent rolling-resistance descriptor and rut depth decreased relative to matched-control dynamics. This confirms that the subsequent operational effects have an independent road base.

3. Difference-in-differences evaluation in matched-control before–after windows showed a consistent reduction in fuel consumption of trips that passed through the analyzed problem segments by 10.6 L/cycle, a reduction in cycle time by 0.78 min, an increase

in focus segment speed by 10.7 km/h, a decrease in RMS vibration by 0.351 g and a decrease in suspension-stress proxy by 78.2 MPa-eq. These effects are local intervention-window estimates and should not be transferred to the entire road network without calibration.

4. Event-time diagnostics, a 14-day lead-placebo check, segment-specific estimates, cohort-weighted group-time ATT and the 1 Hz telemetry subset showed that the pooled effect is not attributable to one extreme segment, a simple post-period level difference or a negative-weight staggered-treatment comparison. Pre-trend and placebo checks remain diagnostics rather than proof of unobserved counterfactual equality.

5. Reliability output is limited by reliability-related mechanical-load risk, expressed in terms of vibration RMS, suspension-stress proxy, mechanical-load proxy, and road-sensitive maintenance-event intensity. Direct proof of a decrease in hazard rate, MTBF, or long-term failure requires a separate seasonal array of failures by node.

6. The engineering contribution is a maintenance-priority procedure based on measurable fuel, time and mechanical-load penalties rather than visual road condition alone. The 0.78 min/cycle reduction corresponds to 8.2% of the intervention-before mean and, under the base scenario, approximately 47.5 truck-hours/year; the 10.6 L/cycle fuel effect corresponds to about 38,700 L/year. These values are site-specific scenario consequences and require local calibration.

Future research should combine multi-mine external validation, component-level survival analysis and repeated post-repair monitoring with AI-supported anomaly detection and a mine digital-twin architecture. Microseismic data may be integrated as a complementary rock-mass-instability layer, while road-condition, truck-response and maintenance-effect models remain separately identifiable. This extension would permit transition from short-window mechanical-load-risk evidence to a validated life-cycle reliability and hazard-management framework.

Author Contributions: Conceptualization, A.T.S., A.Y.U. and B.V.M.; methodology, B.V.M. and N.V.M.; validation, I.N.S. and N.V.M.; formal analysis, B.V.M. and A.B.O.; investigation, A.T.S., A.Y.U. and I.N.S.; data curation, I.N.S. and N.V.M.; writing—original draft preparation, B.V.M. and A.Y.U.; writing—review and editing, A.T.S., A.B.O. and N.V.M.; visualization, I.N.S. and B.V.M.; supervision, A.T.S. and BVM. All authors have read and agreed to the published version of the manuscript.

Funding: This research was funded by the Science Committee of the Ministry of Science and Higher Education of the Republic of Kazakhstan (Grant No. AP23489685).

Institutional Review Board Statement: Not applicable.

Informed Consent Statement: Not applicable.

Data Availability Statement: The data presented in this study are available from the corresponding authors upon reasonable request.

Conflicts of Interest: The authors declare no conflicts of interest.

Abbreviations

RCI—Road Condition Index; IRI—International Roughness Index; RR descriptor—apparent rolling-resistance descriptor; UAV—unmanned aerial vehicle; LiDAR—light detection and ranging; VIMS—vehicle information management system; RMS—root mean square; DiD—difference-in-differences; FE—fixed effects; WB—wild bootstrap; MLI—mechanical-load index; MPa-eq.—equivalent stress-proxy scale; CI—confidence interval.

References

1. Dindarloo, S.R.; Siami-Irdemoosa, E. Determinants of Fuel Consumption in Mining Trucks. *Energy* **2016**, *112*, 232–240. [CrossRef]
2. Siami-Irdemoosa, E.; Dindarloo, S.R. Prediction of Fuel Consumption of Mining Dump Trucks: A Neural Networks Approach. *Appl. Energy* **2015**, *151*, 77–84. [CrossRef]
3. Golbasi, O.; Kina, E. Haul Truck Fuel Consumption Modeling under Random Operating Conditions: A Case Study. *Transp. Res. Part D Transp. Environ.* **2022**, *102*, 103135. [CrossRef]
4. Bodziony, P.; Patyk, M. The Influence of the Mining Operation Environment on the Energy Consumption and Technical Availability of Truck Haulage Operations in Surface Mines. *Energies* **2024**, *17*, 2654. [CrossRef]
5. Coffey, J.; Nikraz, H.; Leek, C. Haul Road Rolling Resistance and Pavement Condition. *Aust. J. Civ. Eng.* **2018**, *16*, 12–22. [CrossRef]
6. Coffey, J.; Nikraz, H.; Leek, C. Energy Consumption in Mine Haulage Due to Road Pavement Performance. *Min. Technol.* **2019**, *128*, 106–117. [CrossRef]
7. Medinac, F.; Bamford, T.; Hart, M.; Kowalczyk, M.; Esmaeili, K. Haul Road Monitoring in Open Pit Mines Using Unmanned Aerial Vehicles: A Case Study at Bald Mountain Mine Site. *Min. Metall. Explor.* **2020**, *37*, 1877–1883. [CrossRef]
8. Kim, H.; Lee, W.-H.; Lee, C.-H.; Kim, S.-M. Development of Monitoring Technology for Mine Haulage Road through Sensor-Connected Digital Device and Smartphone Application. *Appl. Sci.* **2022**, *12*, 12166. [CrossRef]
9. Park, S.; Choi, Y. Applications of Unmanned Aerial Vehicles in Mining from Exploration to Reclamation: A Review. *Minerals* **2020**, *10*, 663. [CrossRef]
10. Alegre, D.; de Lemos Peroni, R.; da Rosa Aquino, E.; Dille, F. A Method to Assess Haul Roads Rolling Resistance Using Dispatch System Data. *Min. Technol.* **2021**, *130*, 176–187. [CrossRef]
11. Sime, M.; Bailey, G.; Hajj, E.Y.; Chkaiban, R. Impact of Pavement Roughness on Fuel Consumption for a Range of Vehicle Types. *J. Transp. Eng. Part B Pavements* **2021**, *147*, 04021022. [CrossRef]
12. Kim, R.E.; Kang, S.; Spencer, B.F.; Al-Qadi, I.L.; Ozer, H. Impact of Pavement Roughness and Deflection on Fuel Consumption Using Energy Dissipation. *J. Eng. Mech.* **2019**, *145*, 04019080. [CrossRef]
13. Louhghalam, A.; Akbarian, M.; Ulm, F.-J. Roughness-Induced Pavement–Vehicle Interactions: Key Parameters and Impact on Vehicle Fuel Consumption. *Transp. Res. Rec.* **2015**, *2525*, 62–70. [CrossRef]
14. Nakousi, C.; Pascual, R.; Anani, A.; Kristjanpoller, F.; Lillo, P. An Asset-Management Oriented Methodology for Mine Haul-Fleet Usage Scheduling. *Reliab. Eng. Syst. Saf.* **2018**, *180*, 336–344. [CrossRef]
15. Bodziony, P.; Krysa, Z.; Patyk, M. Operational Environment Effects on Energy Consumption and Reliability in Mine Truck Haulage. *Energies* **2025**, *18*, 3022. [CrossRef]
16. Ranyal, E.; Sadhu, A.; Jain, K. Road Condition Monitoring Using Smart Sensing and Artificial Intelligence: A Review. *Sensors* **2022**, *22*, 3044. [CrossRef] [PubMed]
17. Sattar, S.; Li, S.; Chapman, M. Road Surface Monitoring Using Smartphone Sensors: A Review. *Sensors* **2018**, *18*, 3845. [CrossRef] [PubMed]
18. Choi, Y. Applications of Unmanned Aerial Vehicle and Artificial Intelligence Technologies in Mining from Exploration to Reclamation. *Minerals* **2023**, *13*, 382. [CrossRef]
19. Chand, K.; Bhat, M.F.; Koner, R.; Fissha, Y.; Cheepurupalli, N.R.; Saidani, T.; Ikeda, H. Open-Pit Mine Reclamation Monitoring and Management for a Sustainable Future Using Drone Technology: A Review. *Drones* **2025**, *9*, 601. [CrossRef]
20. Nobahar, P.; Xu, C.; Dowd, P.; Shirani Faradonbeh, R. Exploring Digital Twin Systems in Mining Operations: A Review. *Green Smart Min. Eng.* **2024**, *1*, 474–492. [CrossRef]
21. Rojas, L.; Peña, Á.; Garcia, J. AI-Driven Predictive Maintenance in Mining: A Systematic Literature Review on Fault Detection, Digital Twins, and Intelligent Asset Management. *Appl. Sci.* **2025**, *15*, 3337. [CrossRef]
22. Luan, B.; Zhou, W.; Ao, Z.; Han, Z.; Xiao, Y. Fuel-Efficient Road Classification Methodology for Sustainable Open Pit Mining. *Appl. Sci.* **2025**, *15*, 6309. [CrossRef]
23. Pryalukhin, A.F.; Martyushev, N.V.; Malozyomov, B.V.; Klyuev, R.V.; Filina, O.A.; Konyukhov, V.Y.; Makarov, A.A. Improvement of Operational Reliability of Units and Elements of Dump Trucks Taking into Account the Least Reliable Elements of the System. *World Electr. Veh. J.* **2024**, *15*, 365. [CrossRef]
24. Pryalukhin, A.F.; Martyushev, N.V.; Malozyomov, B.V.; Demin, A.Y.; Pogrebnoy, A.V.; Kuleshova, E.E.; Valuev, D.V. Statistical Modeling and Forecasting of Operational Reliability of Induction Motors of Mining Dump Trucks. *Mathematics* **2026**, *14*, 706. [CrossRef]
25. Alamdari, S.; Basiri, M.H.; Mousavi, A.; Soofastaei, A. Application of Machine Learning Techniques to Predict Haul Truck Fuel Consumption in Open-Pit Mines. *J. Min. Environ.* **2022**, *13*, 69–85. [CrossRef]

26. Tadubana, G.K.; Sigweni, B.; Ayoung, D.A. Systematic Review on Prediction of Haulage Truck Fuel Consumption in Open-Pit Mines. *Int. J. Min. Reclam. Environ.* **2024**, *38*, 833–850. [CrossRef]
27. Shishkin, P.V.; Malozyomov, B.V.; Martyushev, N.V.; Kondratiev, V.V.; Dorofeev, E.M.; Kononenko, R.V.; Vit'kina, G.Y. Optimization of Energy Balance and Powertrain for Electric Mining Dump Trucks in Coal Mine Reclamation Operations. *World Electr. Veh. J.* **2025**, *16*, 601. [CrossRef]
28. Pryalukhin, A.F.; Malozyomov, B.V.; Martyushev, N.V.; Daus, Y.V.; Konyukhov, V.Y.; Oparina, T.A.; Dubrovin, R.G. Simulation Modeling of Energy Efficiency of Electric Dump Truck Use Depending on the Operating Cycle. *World Electr. Veh. J.* **2025**, *16*, 217. [CrossRef]
29. Nasirinezhad, A.; Stevanovic, D.; Krzanovic, D.; Rahmanpour, M. Model for Optimizing Waste-Haulage Systems in Open-Pit Mines (Trucks vs. IPCC System). *Appl. Sci.* **2025**, *15*, 13148. [CrossRef]
30. Cacciuttolo, C.; Guzmán, V.; Catriñir, P.; Atencio, E.; Komarizadehasl, S.; Lozano-Galant, J.A. Low-Cost Sensors Technologies for Monitoring Sustainability and Safety Issues in Mining Activities: Advances, Gaps, and Future Directions in the Digitalization for Smart Mining. *Sensors* **2023**, *23*, 6846. [CrossRef] [PubMed]
31. Zhou, Y.; Guo, X.; Hou, F.; Wang, J. Review of Intelligent Road Defects Detection Technology. *Sustainability* **2022**, *14*, 6306. [CrossRef]
32. Chu, C.; Wang, L.; Xiong, H. A Review on Pavement Distress and Structural Defects Detection and Quantification Technologies Using Imaging Approaches. *J. Traffic Transp. Eng. Engl. Ed.* **2022**, *9*, 135–150. [CrossRef]
33. Yu, Q.; Fang, Y.; Wix, R. Pavement Roughness Index Estimation and Anomaly Detection Using Smartphones. *Autom. Constr.* **2022**, *141*, 104409. [CrossRef]
34. Sang, Y.; Yu, Q.; Fang, Y.; Vo, V.; Wix, R. Smartphone-Based IRI Estimation for Pavement Roughness Monitoring: A Data-Driven Approach. *IEEE Internet Things J.* **2024**, *11*, 19708–19720. [CrossRef]
35. Alqaydi, S.; Zeiada, W.; El Wakil, A.; Alnaqbi, A.J.; Azam, A. A Comprehensive Review of Smartphone and Other Device-Based Techniques for Road Surface Monitoring. *Eng* **2024**, *5*, 3397–3426. [CrossRef]
36. Shishkin, P.V.; Malozyomov, B.V.; Martyushev, N.V.; Sorokova, S.N.; Efremenkov, E.A.; Valuev, D.V.; Qi, M. Mathematical Logic Model for Analysing the Controllability of Mining Equipment. *Mathematics* **2024**, *12*, 1660. [CrossRef]
37. Botshekan, M.; Roxon, J.; Wanichkul, A.; Chirananthavat, T.; Chamoun, J.; Ziq, M.; Anini, B.; Daher, N.; Awad, A.; Ghanem, W.; et al. Roughness-Induced Vehicle Energy Dissipation from Crowdsourced Smartphone Measurements through Random Vibration Theory. *Data-Cent. Eng.* **2020**, *1*, e17. [CrossRef]
38. Imbens, G.W.; Wooldridge, J.M. Recent Developments in the Econometrics of Program Evaluation. *J. Econ. Lit.* **2009**, *47*, 5–86. [CrossRef]
39. Callaway, B.; Sant'Anna, P.H.C. Difference-in-Differences with Multiple Time Periods. *J. Econom.* **2021**, *225*, 200–230. [CrossRef]
40. Goodman-Bacon, A. Difference-in-Differences with Variation in Treatment Timing. *J. Econom.* **2021**, *225*, 254–277. [CrossRef]
41. Bates, D.; Mächler, M.; Bolker, B.; Walker, S. Fitting Linear Mixed-Effects Models Using lme4. *J. Stat. Softw.* **2015**, *67*, 1–48. [CrossRef]
42. Cameron, A.C.; Gelbach, J.B.; Miller, D.L. Bootstrap-Based Improvements for Inference with Clustered Errors. *Rev. Econ. Stat.* **2008**, *90*, 414–427. [CrossRef]
43. MacKinnon, J.G.; Webb, M.D. Wild Bootstrap Inference for Wildly Different Cluster Sizes. *J. Appl. Econom.* **2017**, *32*, 233–254. [CrossRef]
44. Rahimdel, M.J. Bayesian Network Approach for Reliability Analysis of Mining Trucks. *Sci. Rep.* **2024**, *14*, 3415. [CrossRef] [PubMed]
45. Kristjanpoller, F.; Viveros, P.; Zio, E.; Pascual, R.; Aranda, O. Equivalent Availability Index for the Performance Measurement of Haul Truck Fleets. *Eksploat. Niezawodn. Maint. Reliab.* **2020**, *22*, 583–591. [CrossRef]
46. Senses, S.; Kumral, M. An Optimization-Based Approach to Fleet Reliability and Allocation in Open-Pit Mining. *Decis. Anal. J.* **2025**, *15*, 100583. [CrossRef]
47. Zaker Hossein, A.R.; Sayadi, A.R.; Rahimdel, M.J.; Moradi, M.R. Human Reliability Analysis in Maintenance and Repair Operations of Mining Trucks: A Bayesian Network Approach. *Heliyon* **2024**, *10*, e34765. [CrossRef] [PubMed]
48. Tulegenovich, S.A.; Yerzhankyzy, U.A.; Nikitovich, S.I.; Berikbolovna, O.A.; Malozyomov, B.V.; Martyushev, N.V. Field-Validated Multisensor Assessment of Haul-Road Degradation and Its Association with Fuel-Use Proxy Burden, Dynamic Response, and Transport-Cycle Stability in Open-Pit Mining. *Mining* **2026**, *6*, 49. [CrossRef]
49. Sun, L.; Abraham, S. Estimating Dynamic Treatment Effects in Event Studies with Heterogeneous Treatment Effects. *J. Econom.* **2021**, *225*, 175–199. [CrossRef]
50. Roth, J.; Sant'Anna, P.H.C.; Bilinski, A.; Poe, J. What's Trending in Difference-in-Differences? A Synthesis of the Recent Econometrics Literature. *J. Econom.* **2023**, *235*, 2218–2244. [CrossRef]

51. Wang, J.; Dong, L.; Ji, S. Rock Mass Instability Early Warning Model: A Case Study of a High and Steep Annular Slope Mining Area Using Sen's Slope Trend Analysis. *Tunn. Undergr. Space Technol.* **2025**, *159*, 106514. [CrossRef]
52. Dong, W.X.; Zhang, Q.H.; Wang, X.R.; Dong, H.P.; Wang, C.B.; Wang, S.T. Real-Time Rockburst Warning Using Microseismic Multi-Feature Parameters Based on the PSO-GRNN Model. *Nat. Hazards* **2025**, *121*, 24035–24066. [CrossRef]